arXiv:2112.00757v2 [cond-mat.mes-hall] 9 Jan 2022

Majorana/Andreev crossover and the fate of the topological phase transition in inhomogeneous nanowires

Pasquale Marra[1,2,*] and Angela Nigro[3,4]

[1]*Graduate School of Mathematical Sciences, The University of Tokyo, 3-8-1 Komaba, Meguro, Tokyo, 153-8914, Japan*
[2]*Department of Physics, and Research and Education Center for Natural Sciences, Keio University, 4-1-1 Hiyoshi, Yokohama, Kanagawa, 223-8521, Japan*
[3]*Dipartimento di Fisica "E. R. Caianiello", Università degli Studi di Salerno, 84084 Fisciano (Salerno), Italy*
[4]*Consiglio Nazionale delle Ricerche CNR-SPIN, UOS Salerno, 84084 Fisciano (Salerno), Italy*

(Dated: January 11, 2022)

Majorana bound states (MBS) and Andreev bound states (ABS) in realistic Majorana nanowires setups have similar experimental signatures which make them hard to distinguishing one from the other. Here, we characterize the continuous Majorana/Andreev crossover interpolating between fully-separated, partially-separated, and fully-overlapping Majorana modes, in terms of global and local topological invariants, fermion parity, quasiparticle densities, Majorana pseudospin and spin polarizations, density overlaps and transition probabilities between opposite Majorana components. We found that in inhomogeneous wires, the transition between fully-overlapping trivial ABS and nontrivial MBS does not necessarily mandate the closing of the bulk gap of quasiparticle excitations, but a simple parity crossing of partially-separated Majorana modes (ps-MM) from trivial to nontrivial regimes. We demonstrate that fully-separated and fully-overlapping Majorana modes correspond to the two limiting cases at the opposite sides of a continuous crossover: the only distinction between the two can be obtained by estimating the degree of separations of the Majorana components. This result does not contradict the bulk-edge correspondence: Indeed, the field inhomogeneities driving the Majorana/Andreev crossover have a length scale comparable with the nanowire length, and therefore correspond to a nonlocal perturbation which breaks the topological protection of the MBS.

I. INTRODUCTION

Majorana bound states (MBS) can emerge as topologically protected and spatially-separated zero-energy excitations localized at the opposite ends of a one-dimensional (1D) topological superconductor [1–17]. Their nonabelian exchange statistics [1, 18, 19] may lead to the realization of fault-tolerant quantum computation [20–27]. 1D topological superconductivity can be realized in Majorana nanowires, i.e., proximitized semiconducting nanowires with strong spin-orbit coupling and broken time-reversal symmetry [4–17], in epitaxial 1D semiconductor-superconductor heterostructures [28–30], arrays of magnetic atoms deposited on a conventional superconductor [31–41], or optically-trapped ultracold fermionic atoms coupled to a molecular BEC cloud [42–45].

Quite a few experiments observed signatures compatible with the existence of MBSs in Majorana nanowires, e.g., zero-bias conductance peaks (ZBCP) in extended regions of the phase diagram [46–57] and in multi-terminal devices [58–60], fractional Josephson effect [61–63], and Coulomb blockade spectroscopy [64–68]. However, similar signatures may as well be induced by Andreev bound states (ABS) with zero or near-zero energies appearing in the topologically trivial phase [69–75].

There are several physical mechanisms leading to the emergence of these trivial ABS in Majorana nanowires [76]: random disorder [77–88], localized impurities [86, 89], strong interband coupling [79, 90], and spatial inhomogeneities induced by smooth potentials [82, 86–98], quantum dots [81, 82, 87, 88, 91–107], or partial proximization [81, 82, 87, 91–99, 101–111]. Inhomogeneous potentials naturally arise also in ultracold-atom setups due to the presence of the optical-trap used to confine the atomic cloud [42–45]. Indeed, trivial ABS may exhibit quantized ZBCP virtually indistinguishable from those produced by MBS [82–84, 86, 88, 93, 95, 101, 102, 105, 107], mimic the oscillations of the energy splitting of MBS in some regimes [106, 112], be robust against local perturbations [94, 98], and even exhibit nonabelian braiding statistics [97, 113]. However, whereas MBS are exponentially localized at the edges of the nanowire or, equivalently, at a topological domain wall, ABS are localized anywhere inside the wire, typically near inhomogeneities or impurities, and do not necessarily exhibit exponential localization [88, 94–96, 98].

In a single-band, infinitely long, clean and homogenous Majorana nanowire (i.e., with uniform chemical potential μ, Zeeman field b, and superconducting pairing Δ), the presence/absence of MBS correspond to the realization of the nontrivial/trivial topological phase, separated by a sharp topological quantum phase transition (TQPT) [2, 3]. MBS are described by a nonlocal fermionic state as a superposition of two fully-separated Majorana modes exponentially localized at the opposite edges of the wire, with zero overlap and zero energy, topologically robust against local perturbations, and exhibit an exactly quantized ZBCP $G = 2e^2/h$ at both wire ends. This case is well-described as a "black and white" dichotomy: the wire is either topologically nontrivial $|b| > |b_c| \equiv \sqrt{\mu^2 + \Delta^2}$, with the presence of perfectly self-conjugate, exponentially-localized, and fully-separated Majorana modes with *exactly* zero-energy, or topologically trivial $|b| < |b_c|$, with no energy states below the bulk gap [2, 3]. The two phases are separated by a well-defined TQPT which coincides with the closing of the bulk gap ΔE. We note that, even in clean and homogenous wires, MBS are a limiting case, having zero-energy only for $L \to \infty$: In finite wires $L < \infty$, Ma-

jorana modes hybridize and gain a finite energy [92, 110, 114–117].

Unfortunately, in the laboratory everything is finite, and spatial inhomogeneities, disorder, and impurities are practically unavoidable. These effects produce a rich variety of physical regimes which cannot be described in terms of a "black and white" dichotomy. For instance, the properties of ABS induced by random disorder or localized impurities differ qualitatively from ABS induced by spatial inhomogeneities. Disorder-induced and impurity-induced ABS have small or nearly-zero energy, are localized away from the wire edges, and with ZBCP $G \gtrsim 2e^2/h$ in an extended window of the parameter space, typically without end-to-end correlations [78, 81–83, 86, 88, 89, 105]. They may appear in the topologically trivial phase, even at zero magnetic field. By increasing the magnetic field up to the critical value b_c, the system may or may not reach the nontrivial phase at intermediate or strong disorder regimes [86]. Inhomogeneity-induced ABS instead exhibit small energies oscillating in the magnetic field, are localized near the inhomogeneities, with a nearly-quantized ZBCP which may appear only at one end of the wire [94–96, 98, 101]. They always appear at finite fields, below or above the critical field b_c, and exhibit properties that are somewhat similar to those of topologically nontrivial MBS.

The distinction between MBS and ABS can be understood in terms of spatial separation of the Majorana components. It is a well-known fact that any fermionic mode d can be decomposed as a sum of two Majorana modes $d = \gamma_A + \mathrm{i}\gamma_B$. The case where the two modes γ_A and γ_B are localized at the opposite edges of topologically nontrivial wire of infinite length correspond to topologically protected MBS. On the other hand, the case where the two modes γ_A and γ_B are fully or partially overlapping correspond to subgap ABS or overlapping MBS in short wires. The mutual overlap between the Majorana modes and their susceptibility against local perturbations can be quantified by spatial integrals [94]. It is known that wavefunctions of inhomogeneity-induced ABS show a partial-separation of the Majorana components, and can be connected to topologically nontrivial MBS via a continuous crossover from the trivial $b < b_c$ to the nontrivial regime $b > b_c$ [95, 96, 98]. Moreover, it has been shown recently that there exists a crossover between inhomogeneity-induced ABS and disorder-induced ABS [86]. The presence of these two distinct crossovers may seem paradoxical: inhomogeneity-induced ABS can be continuously transformed into nontrivial MBS or trivial ABS. On top of that, these crossovers may occur with or without a sharp quantum phase transition [81, 92, 104, 118, 119] where trivial ABS detach from the bulk excitation spectrum and gradually approach zero-energy as the magnetic fields increases [92, 94, 95, 97]. Therefore, it is natural to ask, is there a continuous crossover between topologically trivial and topologically nontrivial MBS? If this crossover occurs, what is the fate of the topological phase transition?

To answer these questions, we consider single-band clean Majorana nanowires of finite length L described by the Oreg-Lutchyn model [2, 3] in the presence of spatial inhomogeneities and impurities, and characterize the crossover between topologically trivial impurity-induced ABS, inhomogeneities-induced ABS, and topologically nontrivial MBS. Considering several different potential landscapes, we disentangle the different physical regimes separately in terms of topology, fermion parity crossings, and localization properties of the subgap states. In particular, we define and calculate the global and local topological invariants, local Majorana mass, and the fermion parity, and classify the different regimes of the Majorana wire into three different phases, i.e., the homogeneous topologically trivial phase (TTP), the homogeneous topologically nontrivial phase (TNP), and a topologically inhomogeneous phase (TIP) separating the first two phases. We then characterize the localization and mutual overlap of Majorana modes via the quasiparticle densities, Majorana pseudospin and spin polarizations, density overlaps and transition probabilities. This lead us to distinguish between fully-separated Majorana modes (fs-MM), fully-overlapping Majorana modes (fo-MM), and partially-separated Majorana modes (ps-MM) which interpolate between the first two cases. These different kinds of MM can be characterized by the mutual overlap Ω and transition probability W between their two Majorana components, and expectation values of the Majorana pseudospin.

We find that the Majorana/Andreev crossover from impurity-induced ABS to quasi-MBS [86] and from inhomogeneities-induced ABS (quasi-MBS) to MBS [95, 96, 98] can be described as a transition between the two limiting cases of fs-MM and fo-MM, which can be alternatively viewed as a fusion of two MM into a single Dirac-fermion mode. The MM localize at points where the local Majorana mass becomes close to zero, at the nodes of the local Majorana mass, or at the edges of the wire. The first case is realized in the TTP, where the local Majorana mass is always positive, and fo-MM localize at the minima of the local Majorana mass. The second case is realized in the TIP, where ps-MM localize at the nodes of the local Majorana mass. These ps-MM can become fs-MM if the distance between the Majorana modes approaches infinity. The last case is realized in the TNP, where ps-MM localize at the edges of the wire. These ps-MM become fs-MM in the limit of infinitely long wire. The transition between these different phases do not necessarily correspond to the condition $|b| \equiv \sqrt{\mu^2 + \Delta^2}$, and does not necessarily coincide with the closing and reopening of the bulk gap, but only to the presence of fermion parity crossings of the lowest energy (LE) subgap state. For these reasons, we argue that the ps-MM in the TIP and TTP are indistinguishable from a physical point of view.

II. METHODS

A. Hamiltonian

We consider a Majorana nanowire, i.e., a semiconducting nanowire with strong spin-orbit coupling (e.g., InAs, InSb) in a magnetic field, and proximitized superconductivity induced by a conventional s-wave superconductor (e.g. Al), described

by the Oreg-Lutchyn model

$$H = \left(\frac{p^2}{2m} + \frac{\alpha}{\hbar}\sigma_y p - \mu(x) + b(x)\cdot\sigma_z \right)\tau_z + \Delta(x)\mathrm{i}\sigma_y\tau_x, \tag{1}$$

where $p = -\mathrm{i}\hbar\partial_x$ is the momentum operator, σ_i and τ_i with $i = x, y, z$ the Pauli matrices in spin space and particle-hole space, m the effective mass of the wire, α the spin-orbit coupling strength, $\mu(x)$ the chemical potential, $b(x) = (g/2)\mu_B B(x)$ the Zeeman field in the z-direction (perpendicular to the spin-orbit coupling), and $\Delta(x) \geq 0$ the superconducting pairing due to proximization. A more realistic nanowire model can be obtained via a self-energy term describing the proximitized superconductivity in the wire [120, 121] and solving the resulting Hamiltonian self-consistently. However, self-energy corrections may be neglected since they do not affect the quasiparticle states near zero energy [86]. Moreover, in ultracold-atom setups, the superconducting term depends on the quasiparticle densities, and in that case the corresponding Bogoliubov-de Gennes equations needs to be solved self-consistently [42–45].

Notice that the Hamiltonian is real, and consequently its eigenstates have real wavefunctions (up to a global phase). The Hamiltonian is indeed in the BDI symmetry class [122–125] with unbroken particle-hole symmetry $\mathcal{C} = \tau_x\mathcal{K}$ and unbroken "time-reversal" symmetry $\mathcal{T}' = \mathcal{K}$, where $\mathcal{K}$ is the complex conjugate operator. We consider a InSb/Al Majorana wire of length $L = 2000$ nm, $m = 0.015\, m_e \approx 7700\ \mathrm{eV}/c^2$, $\alpha = 0.5$ eV, $b/B = 1.5$ meV/T (i.e., g-factor $g \approx 50$), $\Delta(x) = \Delta = 1$ meV (see Ref. 13). We discretize the continuous Hamiltonian into a tight-binding Hamiltonian via finite-difference method on a discrete lattice with lattice constant $a = 10$ nm and calculate the energy spectra and the density of states (DOS) numerically via exact diagonalization. The code used for the numerical calculations can be found on Zenodo [126].

B. Quasiparticle densities

To determine the localization of Majorana modes along the wire, we discretize the Hamiltonian in Eq. (1) and diagonalize it to obtain the full energy spectra. In particular we focus on the subgap energy level and the corresponding wavefunctions, described in terms of the Nambu bi-spinor

$$\psi(x) = \begin{pmatrix} u_\uparrow(x) \\ u_\downarrow(x) \\ v_\uparrow(x) \\ v_\downarrow(x) \end{pmatrix}. \tag{2}$$

We then calculate the quasiparticle density $\rho(x)$ as the sum of the densities of the particle and hole sectors, i.e.,

$$|\psi(x)|^2 = \sum_{\sigma=\uparrow\downarrow} |u_\sigma(x)|^2 + |v_\sigma(x)|^2. \tag{3}$$

To disentangle the Majorana/Andreev nature of subgap states, we need to look to the quasiparticle density in the Majorana basis. Any fermionic state c can be decomposed into two Majorana modes $c = (\gamma_A + \mathrm{i}\gamma_B)/\sqrt{2}$ with $\gamma_A = (c^\dagger + c)/\sqrt{2}$ and $\gamma_B = (c^\dagger - c)/\sqrt{2}\mathrm{i}$. Hence, the fermionic states in Eq. (2) can be decomposed into two Majorana components (compare with, e.g., Ref. [94]) given by

$$\psi_A(x) = \frac{1}{\sqrt{2}}(\mathbb{1} + \mathcal{C})\psi(x) = \frac{1}{\sqrt{2}} \begin{pmatrix} u_\uparrow(x) + \overline{v}_\uparrow(x) \\ u_\downarrow(x) + \overline{v}_\downarrow(x) \\ v_\uparrow(x) + \overline{u}_\uparrow(x) \\ v_\downarrow(x) + \overline{u}_\downarrow(x) \end{pmatrix}, \tag{4a}$$

$$\psi_B(x) = \frac{1}{\mathrm{i}\sqrt{2}}(\mathbb{1} - \mathcal{C})\psi(x) = \frac{1}{\mathrm{i}\sqrt{2}} \begin{pmatrix} u_\uparrow(x) - \overline{v}_\uparrow(x) \\ u_\downarrow(x) - \overline{v}_\downarrow(x) \\ v_\uparrow(x) - \overline{u}_\uparrow(x) \\ v_\downarrow(x) - \overline{u}_\downarrow(x) \end{pmatrix}. \tag{4b}$$

We then calculate the densities of the two Majorana components as

$$|\psi_A(x)|^2 = \sum_{\sigma=\uparrow\downarrow} |u_\sigma(x) + \overline{v}_\sigma(x)|^2, \tag{5a}$$

$$|\psi_B(x)|^2 = \sum_{\sigma=\uparrow\downarrow} |u_\sigma(x) - \overline{v}_\sigma(x)|^2, \tag{5b}$$

which can be thought as the "partial" quasiparticle density with respect to the two Majorana flavors A and B, with $|\psi(x)|^2 = (|\psi_A(x)|^2 + |\psi_B(x)|^2)/2$.

For fs-MM, we expect two density peaks localized at the opposite ends of the wire, with the two Majorana components fully separated, i.e., with $|\psi_A(x)|^2 = |\psi(x)|^2$ and $|\psi_B(x)|^2 = 0$ on one edge, and $|\psi_B(x)|^2 = |\psi(x)|^2$ and $|\psi_A(x)|^2 = 0$ on the opposite edge. On the other hand, for fo-MM, we naturally expect $|\psi_A(x)|^2 = |\psi_B(x)|^2 = |\psi(x)|^2$, i.e., the two components of the Majorana modes are fully overlapping.

C. Majorana pseudospin

Following Refs. 127 and 128 we define the Majorana pseudospin operator $\mathbf{T} = \boldsymbol{\tau}/2$ as the analogous of the spin operator $\mathbf{S} = \boldsymbol{\sigma}/2$. The expectation values of the Majorana pseudospin are given by $\langle \mathbf{T}(x) \rangle = \langle \psi(x) | \mathbf{T} | \psi(x) \rangle$ with cartesian components given by

$$\langle T_x(x) \rangle = \sum_{\sigma=\uparrow\downarrow} \mathrm{Re}\left(\overline{u}_\sigma(x) v_\sigma(x)\right), \tag{6a}$$

$$\langle T_y(x) \rangle = \sum_{\sigma=\uparrow\downarrow} \mathrm{Im}\left(\overline{u}_\sigma(x) v_\sigma(x)\right), \tag{6b}$$

$$\langle T_z(x) \rangle = \sum_{\sigma=\uparrow\downarrow} \frac{1}{2}\left(|u_\sigma(x)|^2 - |v_\sigma(x)|^2\right), \tag{6c}$$

The expectation values of the x, y components of the Majorana pseudospin coincide with the Majorana polarization introduced in Ref. 129. Notice also that, since the Hamiltonian

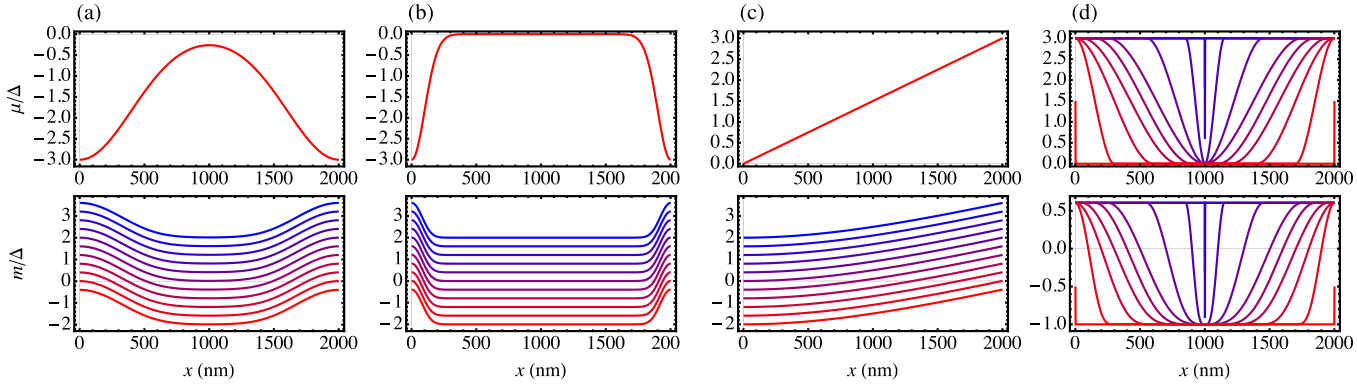


FIG. 1. Spatial dependence of the chemical potential and resulting Majorana mass for different shapes of the potential. (a) and (b) smooth potential barriers in Eq. (18) respectively for $w = 0.2L$ (a) and $w = 0.05L$ for different choices of the magnetic field $0 \leq b \leq 2\Delta$, (c) linear slope in Eq. (19) for different choices of the magnetic field $0 \leq b \leq 2\Delta$, and (d) smoothly interpolating potential defined in Eqs. (21) and (23) for different choices of the control parameter $0 \leq r \leq 4$.

in Eq. (1) and its eigenstates are real, one has $\langle T_y(x)\rangle = 0$. From Eqs. (3) and (7) it follows that

$$|\psi_A(x)|^2 = |\psi(x)|^2 + 2\langle T_x(x)\rangle, \tag{7a}$$
$$|\psi_B(x)|^2 = |\psi(x)|^2 - 2\langle T_x(x)\rangle, \tag{7b}$$

For fs-MM, we expect $\langle T_z(x)\rangle = 0$ and $\langle T_x(x)\rangle \neq 0$ at the edges of the wire, with $\langle T_x(x)\rangle > 0$ and $\langle T_x(x)\rangle < 0$ at opposite edges. Conversely, for fo-MM, we expect $\langle T_x(x)\rangle = 0$ and $\langle T_z(x)\rangle > 0$ for particle-like excitations, and $\langle T_z(x)\rangle < 0$ for hole-like excitations. Hence, Dirac-fermion excitations (i.e., non Majorana) have Majorana pseudospin on the z axis, while Majorana-like excitations have pseudospin perpendicular to the z axis. Since for fs-MM one has that $\langle T_x(x)\rangle > 0$ and $\langle T_x(x)\rangle < 0$ at opposite edges, the average pseudospin along the wire is zero. However, the average of the square of the pseudospin, defined as

$$\langle T_i^2\rangle = \int \mathrm{d}x \, \langle T_i(x)\rangle^2 \tag{8}$$

with $i = x, y, z$, is expected to be nonzero for a fs-MM.

For comparison, we also calculate the expectation values of the spin $\langle \mathbf{S}(x)\rangle = \langle\psi(x)|\,\mathbf{S}\,|\psi(x)\rangle$ with cartesian components given by

$$\langle S_x(x)\rangle = \sum_{w=u,v} \mathrm{Re}\left(\overline{w}_\uparrow(x) w_\downarrow(x)\right), \tag{9a}$$
$$\langle S_y(x)\rangle = \sum_{w=u,v} \mathrm{Im}\left(\overline{w}_\uparrow(x) w_\downarrow(x)\right), \tag{9b}$$
$$\langle S_z(x)\rangle = \sum_{w=u,v} \frac{1}{2}\left(|w_\uparrow(x)|^2 - |w_\downarrow(x)|^2\right). \tag{9c}$$

To characterize the overall spin polarization of subgap modes, we consider the quantities

$$\langle S_i^2\rangle = \int \mathrm{d}x \, \langle S_i(x)\rangle^2, \tag{10}$$

with $i = x, y, z$.

D. Overlaps and matrix elements

We can characterize the mutual overlaps of the Majorana modes in terms of the overlaps of the quasiparticle densities and the matrix elements of the Hamiltonian between the Majorana components. Assuming a single subgap energy level, the overlaps between quasiparticle densities of the Majorana components are

$$\Omega = \int \mathrm{d}x \, |\psi_A(x)||\psi_B(x)|, \tag{11}$$

introduced in Ref. 94. Moreover, the transition probabilities between the two Majorana modes are given by their matrix element

$$W = -\mathrm{i}\int \mathrm{d}x \, \overline{\psi}_A(x) H \psi_B(x). \tag{12}$$

The matrix elements allows one to construct the effective Hamiltonian

$$H_{\text{eff}} = \mathrm{i}W\gamma_A\gamma_B = \frac{1}{2}\begin{pmatrix}\gamma_A & \gamma_B\end{pmatrix}\begin{pmatrix}0 & \mathrm{i}W \\ -\mathrm{i}W & 0\end{pmatrix}\begin{pmatrix}\gamma_A \\ \gamma_B\end{pmatrix}, \tag{13}$$

which describes the low-energy spectra of the Majorana wire in the limit where the energy of the subgap modes are small compared with the bulk gap $W/\Delta E \approx 0$. For fs-MM, there is no overlap of the quasiparticle densities, which mandates $\Omega = W/\Delta E = 0$. For fo-MM instead, one has $|\psi_A(x)| = |\psi_B(x)|$ which gives $\Omega = 1$ and $W/\Delta E \approx 1$.

E. Global topological invariant and fermion parity

In the case of uniform fields, the $\mathbb{Z}_2$ topological invariant of the Majorana wire is $\mathcal{P} = \mathrm{sgn}\,\mathcal{M}$, where $\mathcal{M} = \sqrt{\mu^2 + \Delta^2} - |b|$ is the Majorana mass. Topologically trivial and nontrivial phases are realized respectively for $\mathcal{M} > 0$ and $\mathcal{M} < 0$ [2, 3]. We recall that the lowest energy sector of

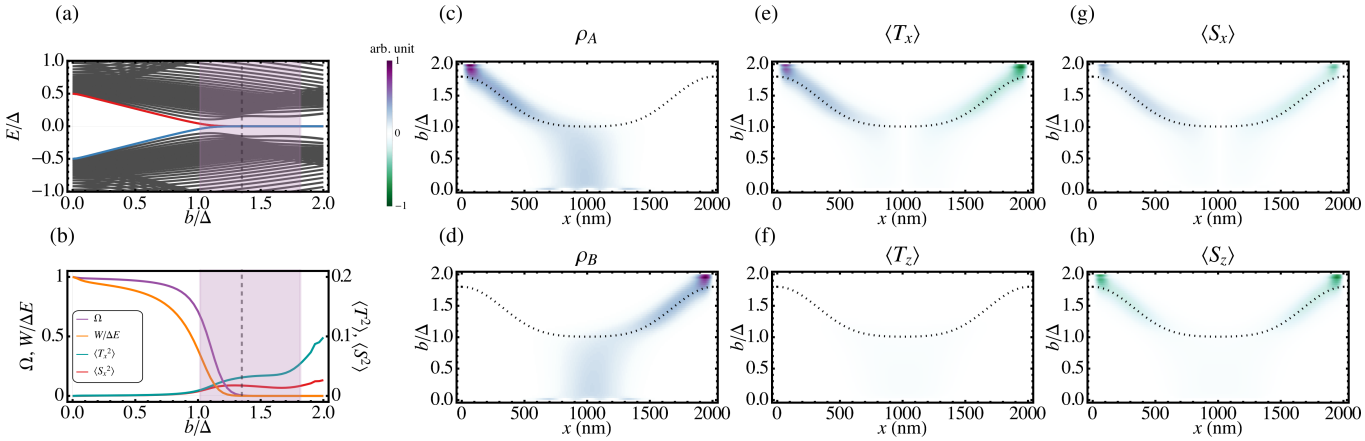


FIG. 2. Numerical results for a Majorana wire with OBC and smooth potential barriers with $w = 0.2L$, as a function of the Zeeman field. (a) Energy spectrum with the two particle-hole symmetric lowest energy (LE) levels highlighted in color. The shaded area corresponds to the topologically inhomogeneous phase (TIP) separating the topologically trivial phase (TTP) and the topologically nontrivial phase (TNP). The vertical line indicates the fermion parity crossing of the groundstate with periodic boundary conditions (PBC). The LE level corresponds to two Majorana modes (MM) which are either fully overlapping (fo-MM) at zero field, or partially-separated (ps-MM). (b) The mutual overlap Ω and transition probability W between the two components of the MM, compared with the expectation values of the square of the Majorana pseudospin $\langle T_x^2\rangle$ and spin $\langle S_x^2\rangle$ integrated along the whole wire. (c), (d) Quasiparticle densities of the two components of the MM as a function of the position, which show a clear spatial separation in the TIP and TNP. (e), (f) Expectation values of the Majorana pseudospin components $\langle T_x(x)\rangle$ and $\langle T_z(x)\rangle$ respectively. (g), (h) Expectation values of the spin components $\langle S_x(x)\rangle$ and $\langle S_z(x)\rangle$ respectively. The peaks of the quasiparticle densities, Majorana pseudospin, and spin, are localized near the nodes of the local Majorana mass (dotted line) in the TIP. The numerical data plotted here and in the following figures can be found on Zenodo [126].

the Oreg-Lutchyn minimal model [2, 3] is unitarily equivalent to a Dirac equation in the Majorana representation and with a Majorana mass equal to $\mathcal{M}$ (see Ref. 130, page 198-202).

In the presence of small inhomogeneities or weak disorder the $\mathbb{Z}_2$ invariant can be generalized [131] as the fermion parity of the groundstate of the system with periodic boundary conditions (PBC). The fermion parity is equal to

$$\mathcal{P} = \operatorname{sgn}\,\operatorname{pf}\left(\mathrm{i}\mathcal{H}\tau_x\right), \tag{14}$$

where the $\mathcal{H}$ is the matrix obtained by discretizing the continuous Hamiltonian H on a discrete lattice. We will calculate the Pfaffian in Eq. (14) numerically [132].

For a finite wire with ps-MM with a finite overlap $W > 0$, the fermion parity of the PBC groundstate is also equal to the sign of the Pfaffian [1] of the effective Hamiltonian in Eq. (13) rewritten in the Majorana basis, which yields

$$\mathcal{P} \equiv \mathcal{P}_{\text{eff}} = \operatorname{sgn}\operatorname{pf}\begin{pmatrix} 0 & W \\ -W & 0 \end{pmatrix} = \operatorname{sgn} W. \tag{15}$$

As a consequence, the transition between trivial and nontrivial topological phase coincide with the fermion parity crossing of the ps-MM (calculated for PBC).

F. Local topological invariant

In the presence of inhomogeneous fields, it makes sense to define a *local* Majorana mass and a *local* topological invariant as

$$m(x) = \sqrt{\mu(x)^2 + \Delta(x)^2} - |b(x)|, \tag{16a}$$
$$p(x) = \operatorname{sgn} m(x). \tag{16b}$$

The local topological invariant of an inhomogeneous system $p(x)$ can be defined in general as the topological invariant of a homogeneous system where all fields are uniform and equal to the values of the fields at the point x. It can be equivalently defined as the topological invariant of a subsystem [133] which coincide with the infinitesimal segment $[x, x + \mathrm{d}x]$. If the spatial variations of the fields are small enough, the local topological invariant is constant along the wire and coincides with the global topological invariant (fermion parity) $p(x) \equiv \mathcal{P}$ in Eq. (14).

However, if spatial variations are large, the local topological invariant may be not constant. In particular, the local Majorana mass may assume alternatively positive and negative values: Segments with $m(x) > 0$ and $m(x) < 0$ realize topologically trivial and nontrivial phases with $p(x) = \pm 1$ respectively. Hence, we distinguish three phases: the homogeneous topologically trivial phase (TTP) where $m(x) > 0$ along the whole wire, the homogeneous topologically nontrivial phase (TNP) where $m(x) < 0$ along the whole wire, and the topologically inhomogeneous phase (TIP) where $m(x)$ changes its sign along the whole wire. A simple criterium to distinguish the homogeneous and inhomogeneous phases is

$$\operatorname{sgn}\left(\min(m(x))\max(m(x))\right) = \begin{cases} +1 \Rightarrow \text{TTP or TNP} \\ -1 \Rightarrow \text{TIP} \end{cases} \tag{17}$$

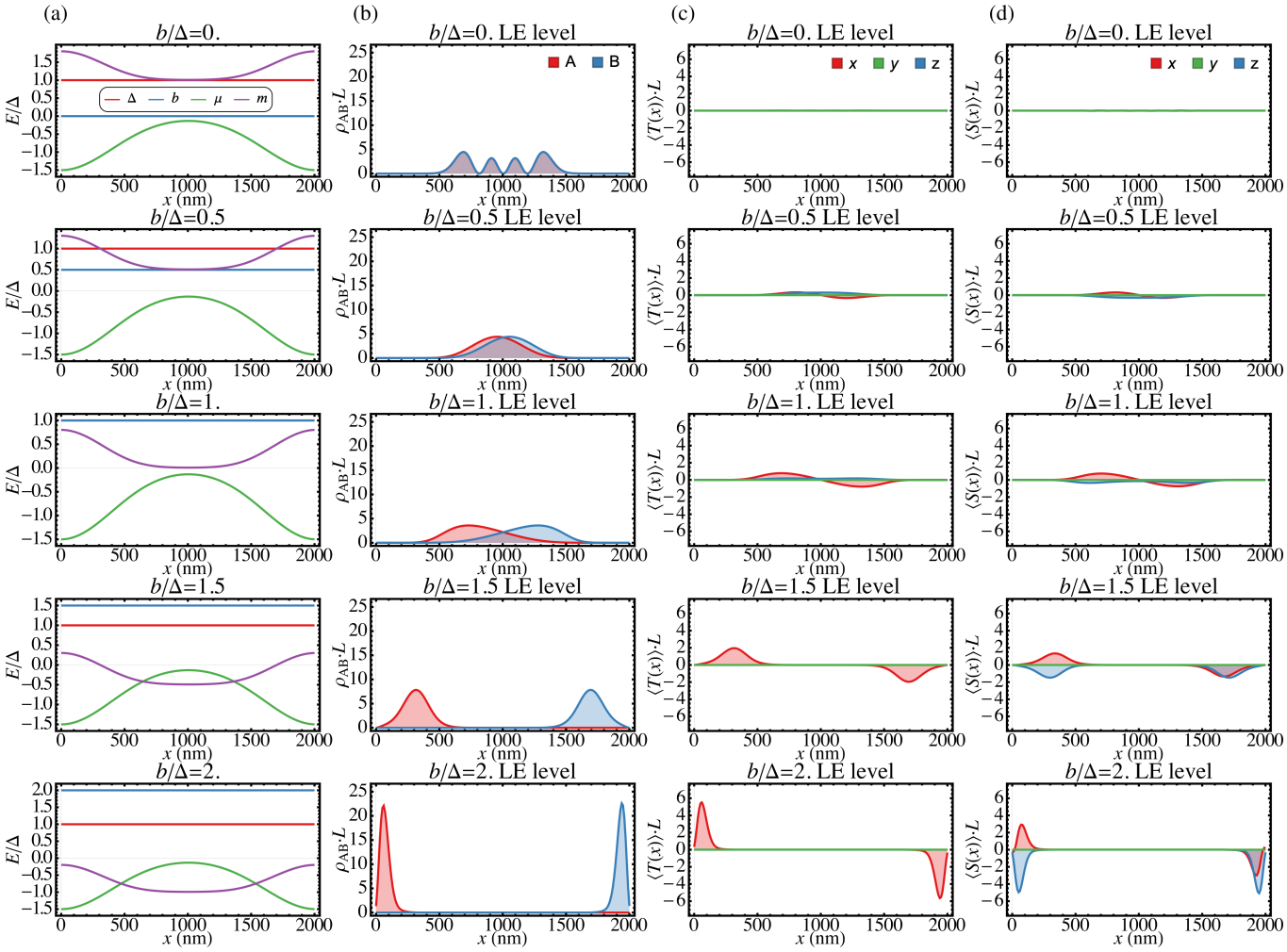


FIG. 3. Snapshots of the numerical results of Fig. 2 at several different Zeeman fields. (a) Chemical potential, Zeeman field, and superconducting pairing, and Majorana mass along the wire. (b) Quasiparticle densities of the two components of the MM. (c), (d) The three components of the Majorana pseudospin and of the spin of the MM.

The fermion parity of the PBC groundstate is even and odd respectively in the TTP and TNP. Consequently, on the intermediate TIP, the subgap levels must exhibit an odd number (at least one) of fermion parity crossings of the PBC groundstate.

In the TIP, assuming that the lengths of the trivial and nontrivial segments are larger than the Majorana localization length $\xi_{\rm M}$, we expect that Majorana modes localize at the boundaries between trivial and nontrivial segments, i.e., at the nodes of the local Majorana mass $m(x) = 0$. If the transition between positive and negative mass $m(x)$ is sufficiently sharp, one may expect that the localization length of the Majorana modes close to the nominal Majorana localization length $\xi_{\rm M}$, which is $\xi \approx \alpha/\Delta$ or $\xi \approx (b/E_{\rm SO})\alpha/\Delta$ respectively for strong and weak spin-orbit coupling regimes $E_{\rm SO} = m\alpha^2/2\hbar^2 \gg \Delta$ and $\ll \Delta$ [12, 114, 119].

G. Fermion parity and topological invariant

One may be tempted to identify the fermion parity of the PBC groundstate as the topological invariant even in the TIP. However, this may not be consistent with the bulk-edge correspondence. To illustrate this, one can consider a simple counterexample of a wire with $\mu = 0$ near the edges $x < L/2$ and $x > 3L/4$ and $\mu = \Delta$ near the center $L/4 < x < 3L/4$. The Majorana mass is consequently $m(x) = \Delta - b$ near the edges and $m(x) = \sqrt{2}\Delta - b$ near the center. For $b < \Delta$ the wire is in the TTP with fermion parity $\mathcal{P} = 1$, for $b > \sqrt{2}\Delta$ it is in the TNP with fermion parity $\mathcal{P} = -1$, whereas for $\Delta < b < \sqrt{2}\Delta$, the wire is in the TIP. Thus, the Majorana mass is $m(x) < 0$ for $x < L/2$ and $x > 3L/4$ (near the edges) and $m(x) > 0$ for $L/4 < x < 3L/4$ (near the center). By increasing the magnetic field b within the TIP, there will necessarily exist a point $b^* < \sqrt{2}\Delta$ where the fermion parity changes its sign, so that $\mathcal{P} = -1$ for $b > b^*$. For values $b^* < b < \sqrt{2}\Delta$, the wire is in the TIP, with the Majorana

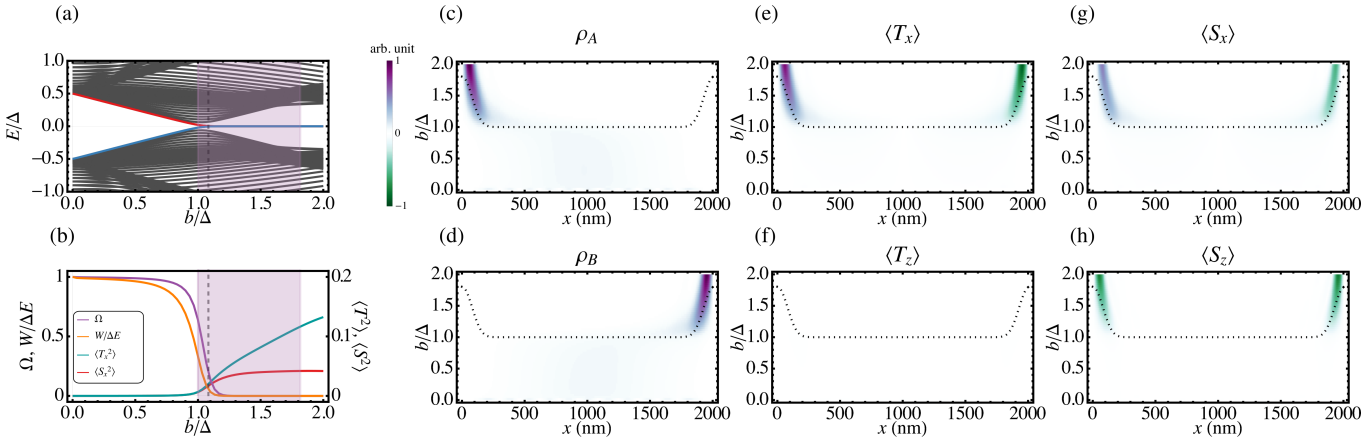


FIG. 4. Numerical results for a Majorana wire with OBC and smooth potential barriers with $w = 0.05L$, as a function of the Zeeman field.

mass changing sign along the wire, and with an odd fermion parity of the PBC. Now, if we impose open boundary conditions (OBC) at $x = 0$ and $x = L$, the wire develops two MM localized at the edges, since $m(x) < 0$ near the edges. Then one can translate the whole wire by $x \to x + L/2$ using PBC. In this second, unitarily equivalent configuration, the wire has still fermion parity $\mathcal{P} = -1$ for $b > b^*$, but there are no MM at the edges, since now one has $m(x) > 0$ near the edges. Therefore, in the TIP, the existence of MM at the edges does not depend on the fermion parity of the PBC groundstate, but only on the value of the local topological invariant near the edges of the wire.

III. RESULTS

A. Crossover via smooth confinement

Potential fluctuation at the end of the nanowire may create inhomogeneous potential barriers. The precise spatial dependence of the resulting potential is usually not known, but can be reasonably approximated as a generic Gaussian-shaped function [82, 88, 95, 97, 98, 113]. We thus consider smooth potential barriers at both edges of the wire, given by

$$\mu(x) = -V(x) = -\delta V \left(\mathrm{e}^{-\frac{x^2}{2w^2}} + \mathrm{e}^{-\frac{(x-L)^2}{2w^2}} \right), \qquad (18)$$

with amplitude $\delta V = 1.5\Delta$ and width $w = 0.05L$ or $w = 0.2L$, and keep the Zeeman field and the superconducting pairing uniform along the wire $b(x) = b$, $\Delta(x) = \Delta$. In this configuration we calculate the energy spectra, fermion parity, and other physical quantities as a function of the magnetic field, for a wire $L = 2000$ nm with OBC. For $b < \Delta$, the wire is in the TTP and the Majorana mass is $m(x) > 0$ along the whole wire. For $\Delta < b < \sqrt{\delta V^2 + \Delta^2}$, the wire is in the TIP with the Majorana mass $m(x) > 0$ in the central section and $m(x) < 0$ near the edges, with the nodes of the Majorana mass given by the solutions of the equation $\sqrt{V(x)^2 + \Delta^2} \equiv b$. For $b > \sqrt{\delta V^2 + \Delta^2}$, the wire reaches the TNP and the Majorana mass is $m(x) < 0$ along the whole wire. The spatial dependence of the chemical potential in Eq. (18) and the resulting Majorana mass for different choices of the magnetic field are shown in Fig. 1(a) and (b) respectively for $w = 0.2L$ and $w = 0.05L$.

Figure 2 shows the energy spectra, the mutual overlap, transition probability, quasiparticle densities, expectation values of the Majorana pseudospin and spin of the MM, calculated for a Majorana wire with OBC and smooth potential barriers with $w = 0.2L$, as a function of the Zeeman field. Figure 3 show snapshots of the quasiparticle densities, expectation values of the Majorana pseudospin and spin of the MM, for different values of the Zeeman field. As the Zeeman field increases, the wire goes from the TTP to the TNP passing by the TIP [shaded areas of Fig. 2(a) and (b)]. A fo-MM detaches from the bulk excitation spectra in TTP and transmutes into a ps-MM at low energy localized at the nodes of the local Majorana mass in the TIP. By increasing the Zeeman field the two MM move continuously from the central region of the wire to the edges, following the nodes of the Majorana mass in the TIP. The peaks in the density, Majorana pseudospin and spin at the nodes have a Gaussian shape, i.e., the MM are smoothly localized at the nodes of the Majorana mass. When the Majorana mass become negative along the whole wire in the TNP, the ps-MM are maximally separated at the two opposite ends of the wire, and become exponentially localized. The crossover from bulk fo-MM into the maximally separated ps-MM occurs in the TIP, with the concurrent change of the fermion parity of the PBC groundstate from $\mathcal{P} = 1$ (TTP and TIP at lower fields) to $\mathcal{P} = -1$ (TNP and TIP at higher fields). This crossover is well captured by the mutual overlaps, transition probabilities, and Majorana pseudospin and spin [see Fig. 2(b)]. The mutual overlap, transition probability are $\Omega, W/\Delta E \approx 1$ for the fo-MM and ps-MM in the TTP, and quickly decays reaching $\Omega, W/\Delta E \approx 0$ already in the TIP at higher Zeeman fields. Conversely, the Majorana pseudospin and spin increase in the TIP. The two components of the ps-MM are separated in space [see Fig. 2(c) and (d)] and the expectation values of the Majorana pseudospin and spin along the x axis have opposite values [see Fig. 2(e) and (g)].

Figures 4 and 5 show the same as before, but smooth poten-

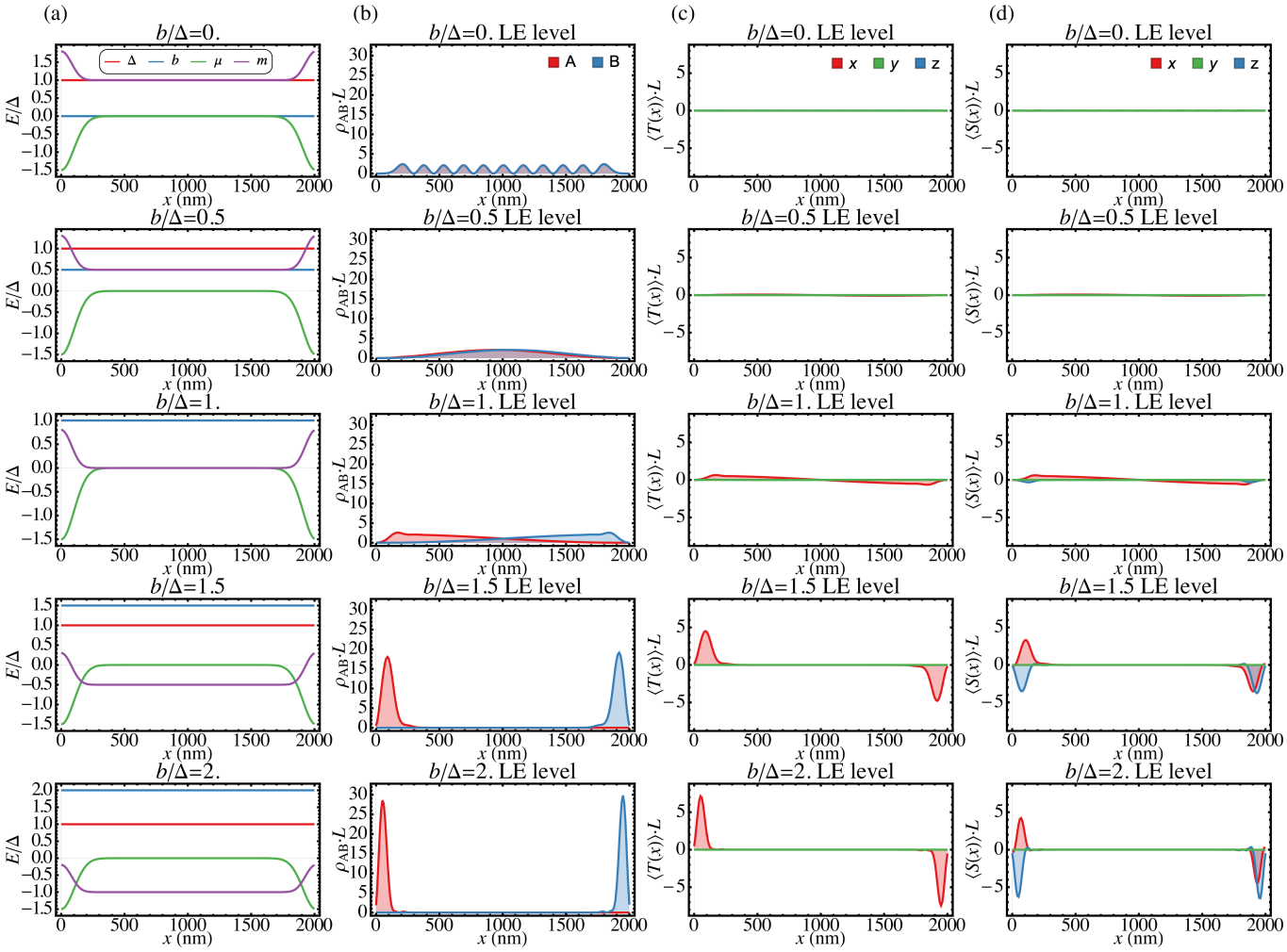


FIG. 5. Snapshots of the numerical results of Fig. 4 at several different Zeeman fields.

tial barriers with $w = 0.05L$. The peaks of the quasiparticle density localized at the nodes of the Majorana mass are much sharper in the case where the width of the Gaussian barrier w is smaller, whereas the peaks are smoothened out in the case of larger w. This indicates a spatial broadening of the ps-MM in the presence of smooth variations of the Majorana mass, and corresponds to a larger overlap between the two components of the ps-MM.

Another relevant feature in the case $w = 0.05L \approx 0$ is that the appearance of the ps-MM at low energy is accompanied by an apparent closing and reopening of the bulk gap [see Fig. 4(a)]. The gap closing correspond at $b = \Delta$ correspond to the presence of a MM localized in an extended region of the wire [see Fig. 5(b)]. However, the closing of the bulk gap is exact only in the limit where the width of the Gaussian barriers vanishes $w \to 0$ which correspond to the limit case of a pristine homogeneous nanowire. Indeed, in the previous case $w = 0.2L$ the bulk gap does not completely close [see Fig. 2(a)], and the regime $b = \Delta$ correspond to the presence of a MM localized in a narrow region of the wire [see Fig. 3(b)].

B. Crossover via linear slope

We consider a linear variation of the potential (linear slope) [95, 98], given by

$$\mu(x) = -V(x) = \delta V x/L, \tag{19}$$

with amplitude $\delta V = 1.5\Delta$, and keep the Zeeman field and the superconducting pairing uniform along the wire $b(x) = b$, $\Delta(x) = \Delta$. As before, we calculate the energy spectra, fermion parity, and other physical quantities as a function of the magnetic field, for a wire $L = 2000$ nm. For $b < \Delta$, the wire is in the TTP and the Majorana mass is $m(x) > 0$ along the whole wire. For $\Delta < b < \sqrt{\delta V^2 + \Delta^2}$, the wire is in the TIP with the Majorana mass $m(x) < 0$ in the left section and $m(x) > 0$ in the right section of wire with nodes of the Majorana mass at $x = \pm\sqrt{b^2 - \Delta^2}L/\delta V$, i.e., the solutions of the equation $\sqrt{(\delta V x/L)^2 + \Delta^2} \equiv b$. For $b > \sqrt{\delta V^2 + \Delta^2}$, the wire reaches the TNP with $m(x) < 0$ along the whole wire. The spatial dependence of the chemical potential in Eq. (19) and the resulting Majorana mass for different choices of the magnetic field are shown in Fig. 1(c).

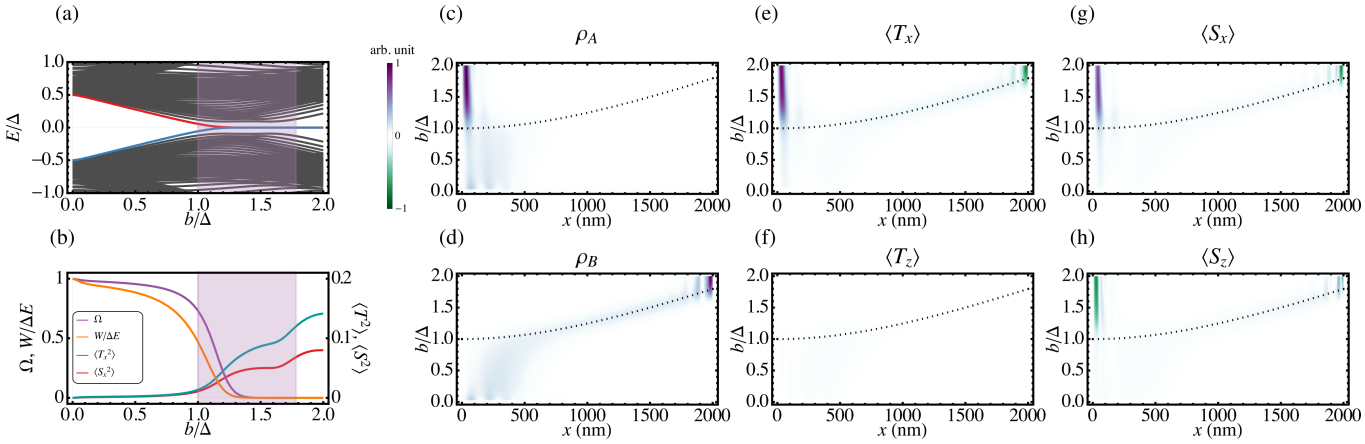


FIG. 6. Numerical results for a Majorana wire with OBC and linear potential slope as a function of the Zeeman field.

Figure 6 shows the energy spectra, the mutual overlap, transition probability, quasiparticle densities, expectation values of the Majorana pseudospin and spin of the MM, calculated for a Majorana wire with OBC and linear slope potential as a function of the Zeeman field. Figure 7 shows instead snapshots for different values of the Zeeman field. As before, the wire goes from the TTP to the TNP passing by the TIP [shaded areas of Fig. 6(a) and (b)] as the Zeeman field increases. Again, a fo-MM detaches from the bulk excitation spectra in TTP and transmutes into a ps-MM at low energy localized near the left edges of the wire: One of the MM become exponentially localized at the left edge as soon as the wire reaches the TIP, whereas a second MM becomes smoothly localized (i.e., with a Gaussian-shape peak) at the node of the local Majorana mass. By increasing the Zeeman field, this second, rightmost MM moves continuously from the left to the right edges, following the node of the Majorana mass in the TIP. Finally, when the wire reaches the TNP, this rightmost MM becomes exponentially localized at the right edge of the wire: the ps-MM is now maximally separated at the two opposite ends of the wire. In this case, we did not calculate the fermion parity of the PBC groundstate, since the linear slope breaks the inversion symmetry between the two edges of the wire and therefore there is no obvious way to impose PBC. As before, the Majorana pseudospin and spin increase, whereas the mutual overlap, transition probability decays from $\Omega, W/\Delta E \approx 1$ in the TTP reaching $\Omega, W/\Delta E \approx 0$ in the TIP at higher Zeeman fields.

In the present case, the peaks of the quasiparticle density localized at the nodes of the Majorana mass are very broad if compared with the results obtained for the smooth potential barriers in the previous section. This is justified by the fact that the potential slope is now linear, and does not exhibit any step-like features. This is compatible with the results of the previous section, where slower variations of the Majorana mass lead to a broader localization peak of the ps-MM.

Moreover, we notice that the bulk gap does not close for any value of the Zeeman field, and the ps-MM simply detaches from the bulk spectra and become gradually pinned at zero energy as the Zeeman field increases.

C. Crossover from impurity-induced ABS to MBS via smoothly interpolating potential

We consider a potential given by the combination of a constant term and a spatially-varying term, as

$$\mu(x) = \mu - V(x), \tag{20}$$

with $\mu = 1.5\Delta$ and

$$V(x) = \delta V \left(S\left(\tfrac{2x-L+d}{2w} + \tfrac{1}{2}\right) - S\left(\tfrac{2x-L-d}{2w} + \tfrac{1}{2}\right)\right), \tag{21}$$

where $S(x)$ is the cubic Hermite interpolator defined by

$$S(x) = \begin{cases} 0 & x < 0 \\ 3x^2 - 2x^3 & 0 \le x \le 1 \\ 1 & x > 1 \end{cases} \tag{22}$$

The potential $V(x)$ is the sum of two smooth step function at a distance d, and interpolates between a localized impurity potential for $d = 0$, $w \to 0$ and a hard wall potential $V(x) \to \delta V(\Theta(x) + \Theta(L-x))$ for $d = L$, $w \to 0$. To obtain a smooth and continuous crossover between these two opposite limits, we vary the parameter $\delta V, w, d$ as a function of a control parameter r as

$$(\delta V, w, d) = \begin{cases} (r\mu, 0, 0) & 0 \le r \le 1, \\ \left(\mu, (r-1)\frac{3L}{8}, (r-1)\frac{3L}{8}\right) & 1 \le r \le 2, \\ \left(\mu, \frac{3L}{8}, (r-2)\frac{L}{4} + \frac{3L}{8}\right) & 2 \le r \le 3, \\ \left(\mu, (4-r)\frac{3L}{8}, (r-3)\frac{3L}{8} + \frac{5L}{8}\right) & 3 \le r \le 4. \end{cases} \tag{23}$$

The evolution of the potential $V(x)$ as a function of the control parameter r and the resulting Majorana mass for $b = 1.5\Delta$ are shown in Fig. 1(d). For $0 < r \le 1$, the potential $V(x)$ is zero with the exception of $x = L/2$ in the middle of the wire, with an increasing peak height $V(L/2) = \delta V = r\mu$.

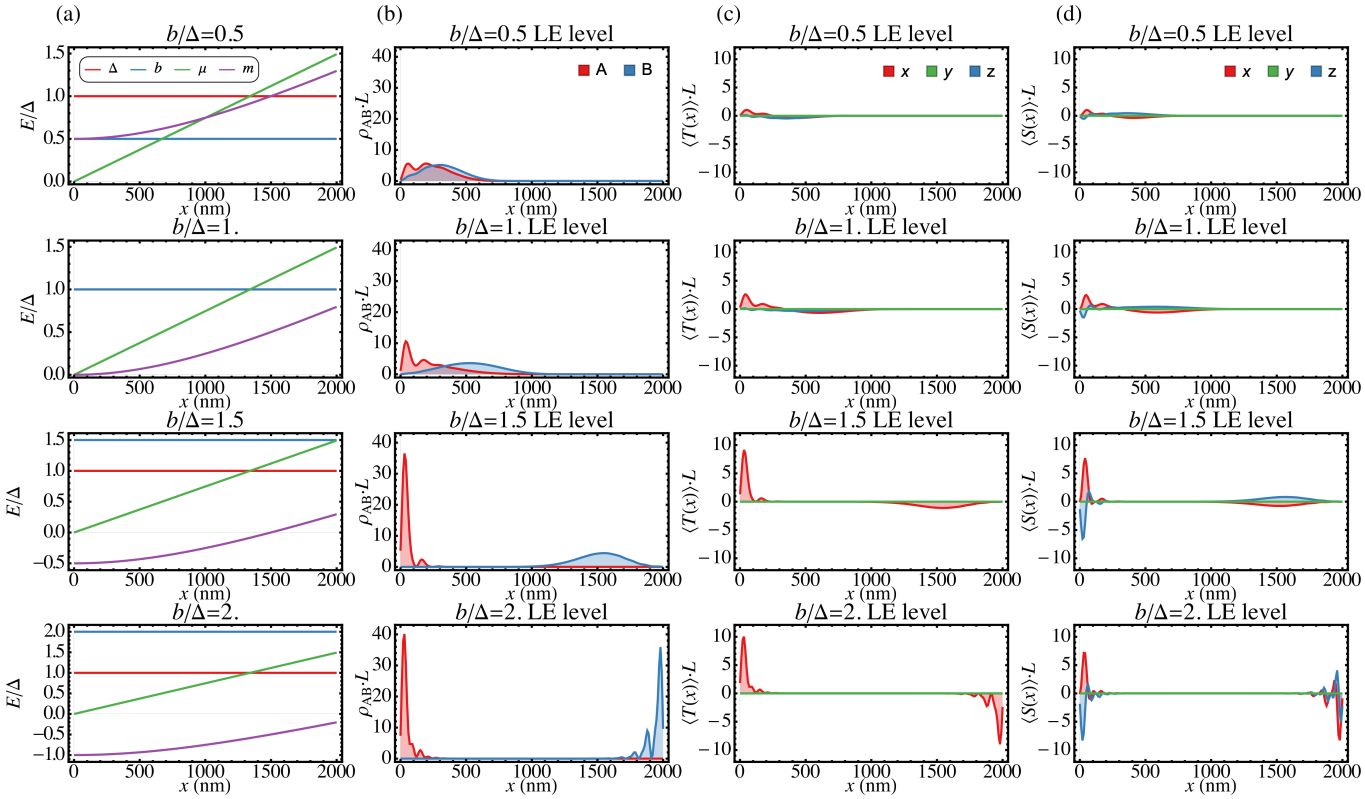


FIG. 7. Snapshots of the numerical results of Fig. 6 at several different Zeeman fields.

This regime models a localized impurity in the centre of the wire. For $1 \leq r \leq 2$, the impurity potential transmutes into a smooth bell-shaped potential. For $2 \leq r \leq 3$, the bell-shaped potential separates into two smooth potential steps at a distance d, gradually reaching the edges of the wire. This regime correspond to smooth inhomogeneous fields at the opposite edges of the wire. For $3 \leq r \leq 4$, the two potential steps at the edges of the wire transition from a smooth potential step into a sharp hard wall potential and becomes constant $V(x) = \delta V$ at $r = 4$. This final regime correspond to a pristine nanowire in the topologically nontrivial phase. The potential $V(x)$ smoothly interpolates between an impurity-like potential ($r = 0$) to the case of a perfectly uniform wire with open boundary conditions in the TNP ($r = 4$) passing through a regime where the potential exhibits smooth spatial variations along the wire. The choice of the interpolation path in Eq. (23) is somewhat arbitrary and not unique, but serves the purpose: Showing the existence of a crossover between impurity-induced ABS and MBS, which can be described as the crossover between fo-MM and fs-MM.

Figure 8 shows the energy spectra, mutual overlap, transition probability, quasiparticle densities, expectation values of the Majorana pseudospin and spin of the MM, calculated for a Majorana wire with OBC with Zeeman field $b = 1.5\Delta$ and $L = 2000$ nm as a function of the interpolation parameter r. Figure 9 shows snapshots for different values of the control parameter r. For small values of the control parameter $r \approx 0$ such that $b < \sqrt{(\mu - \delta V)^2 + \Delta^2}$, the wire is in the TTP and the Majorana mass is $m(x) > 0$ along the whole wire. Increasing $0 \leq r \leq 1$, the potential at $x = L/2$ increases and the central point assumes Majorana mass $m(L/2) < 0$ when $b > \sqrt{(\mu - \delta V)^2 + \Delta^2}$ and the wire enters the TIP [shaded areas of Fig. 8(a) and (b)]. Further increasing $1 \leq r \leq 4$, the wire stays in the TIP with the Majorana mass $m(x) < 0$ in the central section of the wire and $m(x) > 0$ near the edges, with the nodes of the Majorana mass given by the solutions of the equation $\sqrt{V(x)^2 + \Delta^2} \equiv b$. The two MM move continuously from the central region of the wire to the edges, following the nodes of the Majorana mass in the TIP. The whole crossover corresponds to a impurity-induced fo-MM for $r \leq 1$ which gradually transmutes into a inhomogeneities-induced ps-MM at low energy for $r \geq 1$, moving from the center of the wire towards the edges, and smoothly localized (i.e., with a Gaussian-shape peak) at the nodes of the Majorana mass. For $r = 4$, the wire reaches the TNP and the Majorana mass is $m(x) < 0$ along the whole wire, and the two MM become exponentially localized at the edges. Notice that slow variations of the potential lead to a broader localization peak (i.e., Gaussian-like) of the ps-MM, whereas hard-wall potential barriers at $r = 4$ lead to the exponential localization of the MM peaks. As before, the mutual overlap, transition probability decays from $\Omega, W/\Delta E \approx 1$ reaching $\Omega, W/\Delta E \approx 0$ in the TIP at higher fields. Conversely, the Majorana pseudospin and spin show a nearly constant value in the TIP, followed by a fast step-like increase when the MM come closer to the wire edges.

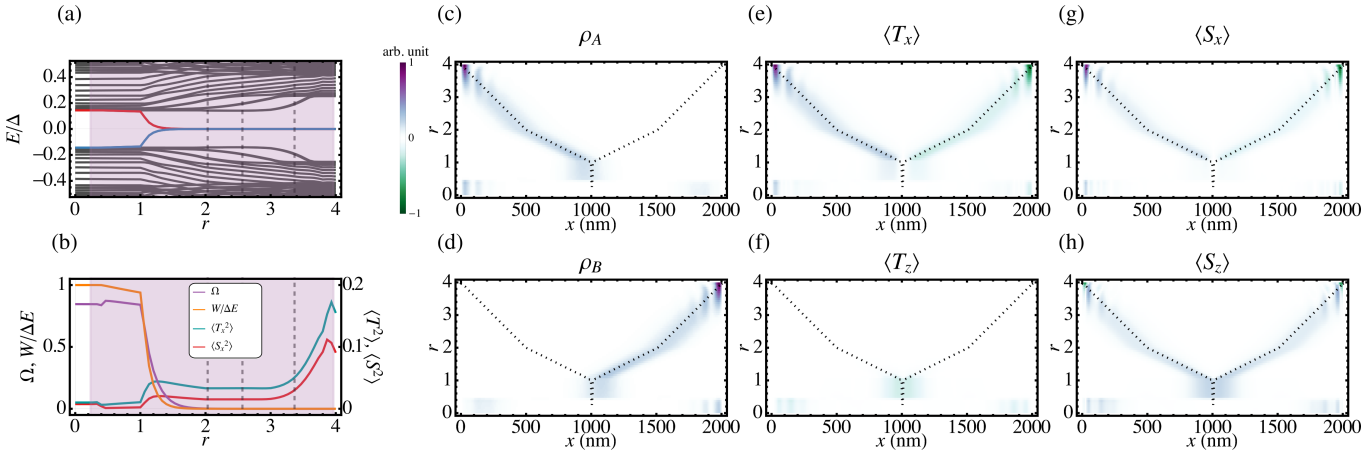


FIG. 8. Numerical results for a Majorana wire with OBC and smoothly interpolating potential as a function of the interpolating parameter r.

The striking feature of the crossover analyzed here is that the bulk gap remains wide open nearly constant during the transition from the TIP into the TNP. This is also true for the energy spectra calculated with PBC. However, the fermion parity of the PBC groundstate shows three parity crossings which amount to the transition from $\mathcal{P} = 1$ at $r \lesssim 2$ to $\mathcal{P} = -1$ for $r \gtrsim 3$. To understand better what happens, we show in Fig. 10 the numerical results calculated for a Majorana wire with PBC as a function of the interpolation parameter r. The PBC energy spectra in the TIP look very similar to the OBC spectra. Notice that even with PBC, there is a ps-MM below the gap, which is localized at the nodes of the Majorana mass in the TIP. This ps-MM is responsible for the fermion parity crossing and eventually, of the transition into the TNP. Thus, the transition to the TNP is not accompanied by the closing and reopening of the bulk gap, but only to a fermion parity transition of a single subgap state. Notice that, when the transition into the TNP is completed, the ps-MM transmutes into a bulk excitation, and there are no localized modes at the edges (as expected for PBC). This corresponds to the fact that the mutual overlap and transition probability decays from $\Omega, W/\Delta E \approx 1$ reaching $\Omega, W/\Delta E \approx 0$ in the TIP and come back to $\Omega, W/\Delta E \approx 1$ in the TNP. Conversely, the Majorana pseudospin and spin show a nearly constant plateau in the TIP, and consequently vanishes in the TNP.

IV. DISCUSSION

We characterized the different physical regimes in terms of topology and localization properties of the subgap states. To characterize topology, we defined and calculated both the global and local topological invariants in the presence of inhomogeneities and impurities, and show how these two quantities differ from the topological invariant of a uniform wire. In particular, three different phases appear: the homogeneous topologically trivial phase (TTP), the homogeneous topologically nontrivial phase (TNP), and a topologically inhomogeneous phase (TIP) separating the first two phases. In the two homogenous phases, the local topological invariant is uniform along the wire, and coincides with the global topological invariant, being either trivial (TTP) or nontrivial (TNP). In the TIP, the local topological invariant is nonuniform along the wire, Majorana modes localize near the points where the local topological invariant changes sign, i.e., at the nodes of the local Majorana mass $m(x)$. Since the fermion parity of the PBC groundstate is even and odd respectively in the TTP and in the TNP, the subgap levels must exhibit an odd number of fermion parity crossing in the TIP. However, the topological transition does not necessarily correspond to the condition $|b| \equiv |b_c| = \sqrt{\mu^2 + \Delta^2}$, and does not necessarily coincide with the closing and reopening of the bulk gap, but only to a parity crossing of the LE subgap state.

To characterize the localization properties of the subgap state, we define and calculate the wavefunctions, quasiparticle densities, Majorana pseudospin and spin polarizations, density overlaps and transition probabilities between the Majorana components. This lead us to distinguish between fully-separated Majorana modes (fs-MM) with $\Omega = W = 0$, partially-separated Majorana modes (ps-MM) with $0 < \Omega < 1$ and $W > 0$, and fully-overlapping Majorana modes (fo-MM) with $\Omega = 1$ and $W \approx \Delta E$. Notice that these definitions are not based on topology, but only on the intrinsic properties of the subgap wavefunctions, and well-defined both for infinite and finite wires. In this context, topologically protected MBS can be unambiguously defined as a couple of fs-MM localized at the opposite ends of an infinite wire in the homogeneous topologically nontrivial phase, or in the inhomogeneous phase with nontrivial global topological invariant, as long as the nodes of the Majorana mass are restricted in a finite segment at a finite distance from the wire edges. Thus, strictly speaking fs-MM are a limiting case which only exists in infinite-size systems. In finite-size wires, only ps-MM and fo-MM can exist.

Any occurrence of Majorana/Andreev crossover can be described as a transition along the continuous interval $\Omega \in [0, 1]$ between the two limiting cases of fs-MM ($\Omega = 0$) and fo-MM ($\Omega = 1$). This crossover can be described as the fusion of two Majorana modes (fs-MM, $\Omega = 0$) localized at the nodes of the Majorana mass $m(x) \equiv 0$ (or at the edges

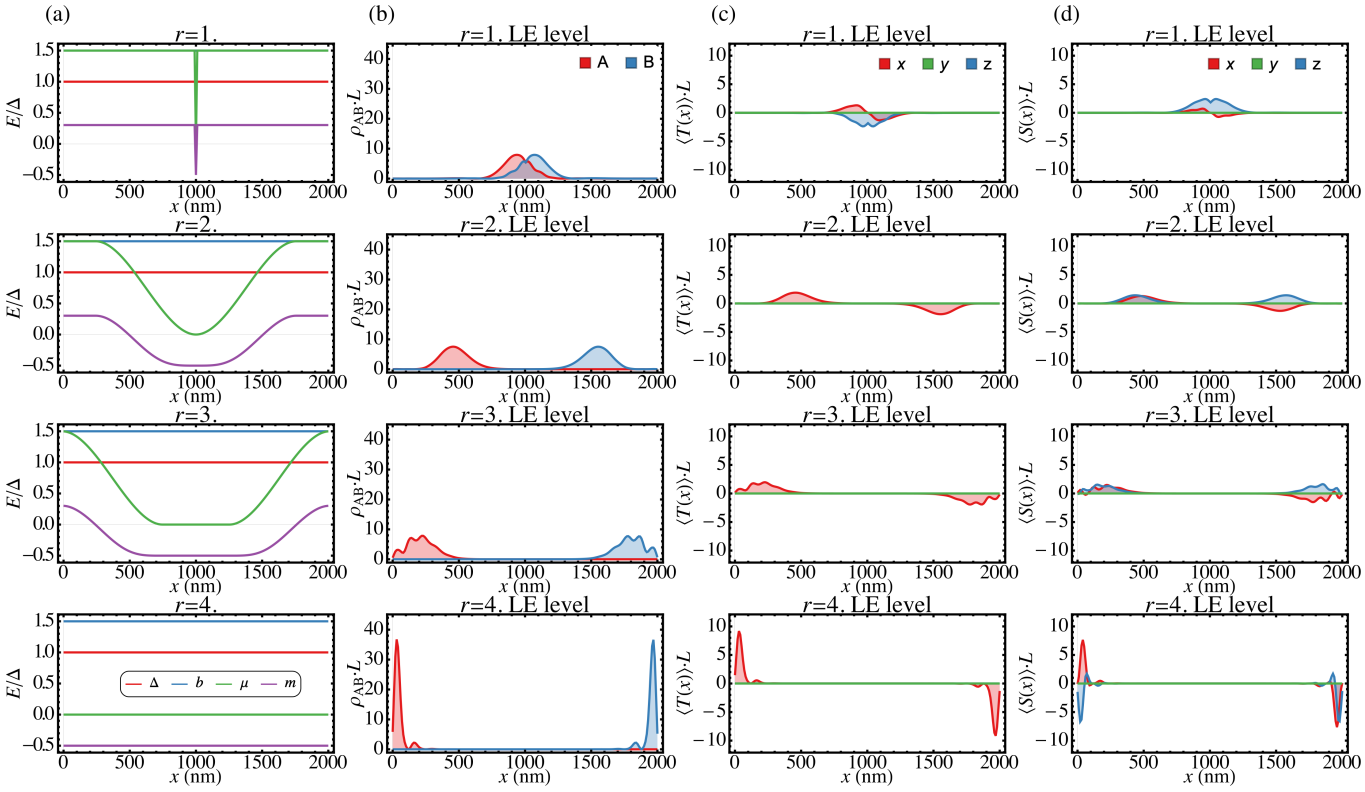


FIG. 9. Snapshots of the numerical results of Fig. 8 at several different values of the interpolating parameter r.

of the wire) into a single Dirac fermion (fo-MM, $\Omega = 1$) when the two nodes become close together, merge, and disappear. The crossover from impurity-induced ABS to quasi-MBS [86] coincides with the crossover from a single fo-MM ($\Omega = 1$) localized around the impurity in the TTP, to a ps-MM ($0 < \Omega < 1$) in the TIP. On the other hand, the crossover from inhomogeneities-induced ABS (quasi-MBS) to MBS [95, 96, 98] coincides with the crossover from a ps-MM ($0 < \Omega < 1$) in the TIP, to a fs-MM ($\Omega = 1$) in the TNP. Finally, there exists a crossover from impurity-induced ABS to topologically-protected MBS, i.e., from a single fo-MM ($\Omega = 1$) localized around the impurity in a TTP, to a fs-MM ($\Omega = 0$) localized at the wire ends in the TNP.

The presence of a continuous crossover between trivial and nontrivial subgap modes without a TQPT suggests that it may be not physically possible to univocally and unambiguously distinguish between "true" MBS, and other varieties of subgap modes. In fact, any subgap mode is characterized by the mutual overlap X of its Majorana components, on a continuous crossover $X \in [0, 1]$ of ps-MM, with the limiting cases of fo-MM with overlap $X = 1$ and fs-MM with $X = 0$. Pragmatically, however, it is still relevant to determine the extent of the spatial separation of the MM, i.e., how well separated are the Majorana components γ_A and γ_B along the wire, where are these components localized, and how robust they are against disorder. The degree of spatial separation between MM and their localization with respect to the wire edges can be determined by nonlocal experiments [82, 87, 89, 95, 97, 102, 105, 134–147].

For brevity, we considered in this work only configurations with only two MM localized inside the wire, corresponding to the presence of only two nodes of the Majorana mass $m(x)$, and we only considered spatial variations of the chemical potential. The results presented here can be easily generalized to cases where both the chemical potential, Zeeman field, and superconducting pairing are spatially modulated along the wire, and to configurations where the Majorana mass exhibit more than two nodes within the wire.

The description of subgap states as partially separated modes localized at the nodes of the Majorana mass is well-suited only for inhomogeneous fields having variations on length scales comparable with the Majorana localization length, and such that the nodes of the Majorana mass correspond to the presence of a few, well-separated subgap modes. This description breaks down, e.g., in the regime of strong disorder [83, 84]. In this case, the Majorana mass may exhibit large oscillations and its nodes may become extremely dense and close to each other, which results in the proliferation of subgap modes hybridized over the whole length of the wire. In this regime, it is not meaningful to model the Majorana nanowire via an effective low-energy Hamiltonian describing the hybridization of a few subgap Majorana modes, as in Eq. (13). The transition between impurity-induced ABS described here and strong disorder is left for future work. Moreover, at very short lengths, the discreteness of the atomic lattice cannot be neglected. This may lead to a quasiperiodic regime where the competition between lattice and field length scales give rise to fractal energy bands (Hofstadter butterfly)

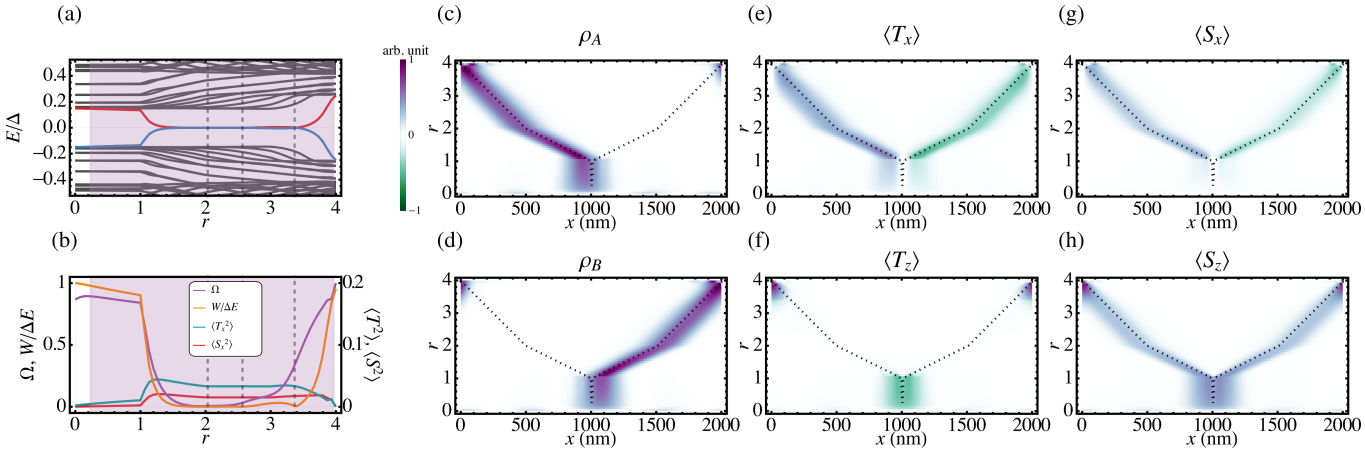


FIG. 10. Numerical results as in Fig. 8 but for a Majorana wire with PBC.

and Anderson localization [148–150], or to the presence of nontrivial ABS [151]. Another example of ABS which cannot be described as separated Majorana modes localized at the nodes of the Majorana mass is the intrinsic ABS described in Ref. [104].

V. CONCLUSIONS

In summary, we characterized the continuous crossover between Andreev and Majorana bound states in terms of their Majorana components, showing how the crossover between impurity-induced to inhomogeneities-induced subgap modes and to Majorana bound states can be described as the crossover between fully-overlapping to partially-separated and fully-separated Majorana modes. The localization of the Majorana modes have been characterized via their quasiparticle density, mutual overlap, transition probability, Majorana pseudospin, and spin polarizations along the wire. We showed that these partially-separated modes localize at the nodes of the Majorana mass, being either exponentially or smoothly localized respectively in the case of sharp and smooth variations of the Majorana mass near the node. In particular, Majorana bound states localized at the wire edges correspond to the limiting case of fully-separated Majorana modes realized when the distance between the Majorana modes is infinite. We discussed the presence of a topological inhomogeneous phase which is intermediate between the topologically trivial and nontrivial phases, and is characterized by a local topological invariant spatially-varying along the wire. We evidenced the absence of a global topological phase transition: Different regimes are still characterized by a different fermion parity. However, changes of the fermion parity do not correspond necessarily to the closing of the particle-hole gap, but may occur via the parity crossing of the lowest energy subgap state. This work suggests that there may be no sharp distinction between "true" Majorana bound states and other varieties of zero-energy or near-zero-energy subgap modes in the presence of spatially-varying potentials and impurities. Indeed, subgap modes in Majorana wires interpolate continuously between fully-overlapping, partially-separated, and fully-separated Majorana modes.

ACKNOWLEDGMENTS

The work of P. M. is supported by the Japan Science and Technology Agency (JST) of the Ministry of Education, Culture, Sports, Science and Technology (MEXT), JST CREST Grant. No. JPMJCR19T2, and by the Japan Society for the Promotion of Science (JSPS) Grant-in-Aid for Early-Career Scientists (Grant No. 20K14375).

DATA AVAILABILITY STATEMENT

The code used for the numerical calculations and the resulting data can be found on Zenodo [126].

* pmarra@ms.u-tokyo.ac.jp

[1] A. Kitaev, Unpaired Majorana Fermions in Quantum Wires, Phys. Usp. **44**, 131 (2001).
[2] Y. Oreg, G. Refael, and F. Von Oppen, Helical Liquids and Majorana Bound States in Quantum Wires, Phys. Rev. Lett. **105**, 177002 (2010).
[3] R. Lutchyn, J. Sau, and S. Das Sarma, Majorana Fermions and a Topological Phase Transition in Semiconductor-Superconductor Heterostructures, Phys. Rev. Lett. **105**, 077001 (2010).
[4] J. Alicea, New Directions in the Pursuit of Majorana Fermions in Solid State Systems, Rep. Prog. Phys. **75**, 076501 (2012).

[5] M. Leijnse and K. Flensberg, Introduction to Topological Superconductivity and Majorana Fermions, Semicond. Sci. Technol. **27**, 124003 (2012).

[6] T. Stanescu and S. Tewari, Majorana Fermions in Semiconductor Nanowires: Fundamentals, Modeling, and Experiment, J. Condens. Matter Phys. **25**, 233201 (2013).

[7] C. Beenakker, Search for Majorana Fermions in Superconductors, Annu. Rev. Condens. Matter Phys. **4**, 113 (2013).

[8] S. Elliott and M. Franz, Colloquium: Majorana Fermions in Nuclear, Particle, and Solid-State Physics, Rev. Mod. Phys. **87**, 137 (2015).

[9] C. Beenakker, Random-Matrix Theory of Majorana Fermions and Topological Superconductors, Rev. Mod. Phys. **87**, 1037 (2015).

[10] M. Sato and S. Fujimoto, Majorana Fermions and Topology in Superconductors, J. Phys. Soc. Japan **85**, 072001 (2016).

[11] M. Sato and Y. Ando, Topological Superconductors: A Review, Rep. Prog. Phys. **80**, 076501 (2017).

[12] R. Aguado, Majorana Quasiparticles in Condensed Matter, Riv. del Nuovo Cim. **40**, 523 (2017).

[13] R. Lutchyn, E. Bakkers, L. Kouwenhoven, P. Krogstrup, C. Marcus, and Y. Oreg, Majorana Zero Modes in Superconductor-Semiconductor Heterostructures, Nat. Rev. Mater. **3**, 52 (2018).

[14] H. Zhang, D. Liu, M. Wimmer, and L. Kouwenhoven, Next Steps of Quantum Transport in Majorana Nanowire Devices, Nat. Commun. **10**, 5128 (2019).

[15] Y. Li and Z.-A. Xu, Exploring Topological Superconductivity in Topological Materials, Adv. Quantum Technol. **2**, 1800112 (2019).

[16] S. Frolov, M. Manfra, and J. Sau, Topological superconductivity in hybrid devices, Nat. Phys. **16**, 718 (2020).

[17] K. Flensberg, F. von Oppen, and A. Stern, Engineered platforms for topological superconductivity and Majorana zero modes, Nat. Rev. Mater. **6**, 944 (2021).

[18] D. Ivanov, Non-Abelian Statistics of Half-Quantum Vortices in p-Wave Superconductors, Phys. Rev. Lett. **86**, 268 (2001).

[19] A. Kitaev, Fault-Tolerant Quantum Computation by Anyons, Ann. Phys. **303**, 2 (2003).

[20] C. Nayak, S. Simon, A. Stern, M. Freedman, and S. Das Sarma, Non-Abelian Anyons and Topological Quantum Computation, Rev. Mod. Phys. **80**, 1083 (2008).

[21] J. K. Pachos, Introduction to Topological Quantum Computation (Cambridge University Press, 2012).

[22] S. D. Sarma, M. Freedman, and C. Nayak, Majorana zero modes and topological quantum computation, npj Quantum Inf. **1**, 15001 (2015).

[23] V. Lahtinen and J. Pachos, A Short Introduction to Topological Quantum Computation, SciPost Phys. **3**, 021 (2017).

[24] T. D. Stanescu, Introduction to topological quantum matter & quantum computation (Taylor & Francis, 2017).

[25] C. W. J. Beenakker, Search for non-Abelian Majorana braiding statistics in superconductors, SciPost Phys. Lect. Notes 15 (2020).

[26] Y. Oreg and F. von Oppen, Majorana Zero Modes in Networks of Cooper-Pair Boxes: Topologically Ordered States and Topological Quantum Computation, Annu. Rev. Condens. Matter Phys. **11**, 397 (2020).

[27] R. Aguado, A perspective on semiconductor-based superconducting qubits, Appl. Phys. Lett. **117**, 240501 (2020).

[28] J. Shabani, M. Kjaergaard, H. Suominen, Y. Kim, F. Nichele, K. Pakrouski, T. Stankevic, R. Lutchyn, P. Krogstrup, R. Feidenhans'L, S. Kraemer, C. Nayak, M. Troyer, C. Marcus, and C. Palmstrøm, Two-Dimensional Epitaxial Superconductor-Semiconductor Heterostructures: A Platform for Topological Superconducting Networks, Phys. Rev. B **93**, 155402 (2016).

[29] M. Hell, M. Leijnse, and K. Flensberg, Two-Dimensional Platform for Networks of Majorana Bound States, Phys. Rev. Lett. **118**, 107701 (2017).

[30] F. Pientka, A. Keselman, E. Berg, A. Yacoby, A. Stern, and B. Halperin, Topological Superconductivity in a Planar Josephson Junction, Phys. Rev. X **7**, 021032 (2017).

[31] T.-P. Choy, J. Edge, A. Akhmerov, and C. Beenakker, Majorana Fermions Emerging from Magnetic Nanoparticles on a Superconductor without Spin-Orbit Coupling, Phys. Rev. B **84**, 195442 (2011).

[32] S. Nadj-Perge, I. Drozdov, B. Bernevig, and A. Yazdani, Proposal for Realizing Majorana Fermions in Chains of Magnetic Atoms on a Superconductor, Phys. Rev. B **88**, 020407 (2013).

[33] F. Pientka, L. Glazman, and F. Von Oppen, Topological Superconducting Phase in Helical Shiba Chains, Phys. Rev. B **88**, 155420 (2013).

[34] B. Braunecker and P. Simon, Interplay between Classical Magnetic Moments and Superconductivity in Quantum One-Dimensional Conductors: Toward a Self-Sustained Topological Majorana Phase, Phys. Rev. Lett. **111**, 147202 (2013).

[35] J. Klinovaja, P. Stano, A. Yazdani, and D. Loss, Topological Superconductivity and Majorana Fermions in RKKY Systems, Phys. Rev. Lett. **111**, 186805 (2013).

[36] M. Vazifeh and M. Franz, Self-Organized Topological State with Majorana Fermions, Phys. Rev. Lett. **111**, 206802 (2013).

[37] J. Li, H. Chen, I. Drozdov, A. Yazdani, B. Bernevig, and A. Macdonald, Topological Superconductivity Induced by Ferromagnetic Metal Chains, Phys. Rev. B **90**, 235433 (2014).

[38] Y. Kim, M. Cheng, B. Bauer, R. Lutchyn, and S. Das Sarma, Helical Order in One-Dimensional Magnetic Atom Chains and Possible Emergence of Majorana Bound States, Phys. Rev. B **90**, 060401 (2014).

[39] F. Pientka, L. Glazman, and F. Von Oppen, Unconventional Topological Phase Transitions in Helical Shiba Chains, Phys. Rev. B **89**, 180505 (2014).

[40] A. Heimes, P. Kotetes, and G. Schön, Majorana Fermions from Shiba States in an Antiferromagnetic Chain on Top of a Superconductor, Phys. Rev. B **90**, 060507 (2014).

[41] P. Brydon, S. Das Sarma, H.-Y. Hui, and J. Sau, Topological Yu-Shiba-Rusinov Chain from Spin-Orbit Coupling, Phys. Rev. B **91**, 064505 (2015).

[42] L. Jiang, T. Kitagawa, J. Alicea, A. R. Akhmerov, D. Pekker, G. Refael, J. I. Cirac, E. Demler, M. D. Lukin, and P. Zoller, Majorana Fermions in Equilibrium and in Driven Cold-Atom Quantum Wires, Phys. Rev. Lett. **106**, 220402 (2011).

[43] S. Nascimbène, Realizing one-dimensional topological superfluids with ultracold atomic gases, J. Phys. B **46**, 134005 (2013).

[44] A. Bühler, N. Lang, C. V. Kraus, G. Möller, S. D. Huber, and H. P. Büchler, Majorana modes and p-wave superfluids for fermionic atoms in optical lattices, Nat. Commun. **5**, 4504 (2014).

[45] A. Ptok, A. Cichy, and T. Domański, Quantum engineering of Majorana quasiparticles in one-dimensional optical lattices, J. Condens. Matter Phys. **30**, 355602 (2018).

[46] V. Mourik, K. Zuo, S. Frolov, S. Plissard, E. Bakkers, and L. Kouwenhoven, Signatures of Majorana Fermions in Hybrid Superconductor-Semiconductor Nanowire Devices, Science **336**, 1003 (2012).

[47] A. Das, Y. Ronen, Y. Most, Y. Oreg, M. Heiblum, and H. Shtrikman, Zero-Bias Peaks and Splitting in an Al-InAs

Nanowire Topological Superconductor as a Signature of Majorana Fermions, Nat. Phys. **8**, 887 (2012).
[48] M. Deng, C. Yu, G. Huang, M. Larsson, P. Caroff, and H. Xu, Anomalous Zero-Bias Conductance Peak in a Nb-InSb Nanowire-Nb Hybrid Device, Nano Lett. **12**, 6414 (2012).
[49] H. Churchill, V. Fatemi, K. Grove-Rasmussen, M. Deng, P. Caroff, H. Xu, and C. Marcus, Superconductor-Nanowire Devices from Tunneling to the Multichannel Regime: Zero-Bias Oscillations and Magnetoconductance Crossover, Phys. Rev. B **87**, 241401 (2013).
[50] A. Finck, D. Van Harlingen, P. Mohseni, K. Jung, and X. Li, Anomalous Modulation of a Zero-Bias Peak in a Hybrid Nanowire- Superconductor Device, Phys. Rev. Lett. **110**, 126406 (2013).
[51] M. Deng, S. Vaitiekenas, E. Hansen, J. Danon, M. Leijnse, K. Flensberg, J. Nygård, P. Krogstrup, and C. Marcus, Majorana Bound State in a Coupled Quantum-Dot Hybrid-Nanowire System, Science **354**, 1557 (2016).
[52] F. Nichele, A. Drachmann, A. Whiticar, E. O'Farrell, H. Suominen, A. Fornieri, T. Wang, G. Gardner, C. Thomas, A. Hatke, P. Krogstrup, M. Manfra, K. Flensberg, and C. Marcus, Scaling of Majorana Zero-Bias Conductance Peaks, Phys. Rev. Lett. **119**, 136803 (2017).
[53] J. Chen, P. Yu, J. Stenger, M. Hocevar, D. Car, S. Plissard, E. Bakkers, T. Stanescu, and S. Frolov, Experimental Phase Diagram of Zero-Bias Conductance Peaks in Superconductor/Semiconductor Nanowire Devices, Sci. Adv. **3**, e1701476 (2017).
[54] M.-T. Deng, S. Vaitiekenas, E. Prada, P. San-Jose, J. Nygård, P. Krogstrup, R. Aguado, and C. Marcus, Nonlocality of Majorana Modes in Hybrid Nanowires, Phys. Rev. B **98**, 085125 (2018).
[55] Ö. Gül, H. Zhang, J. D. S. Bommer, M. W. A. de Moor, D. Car, S. R. Plissard, E. P. A. M. Bakkers, A. Geresdi, K. Watanabe, T. Taniguchi, and L. P. Kouwenhoven, Ballistic Majorana Nanowire Devices, Nature Nanotech. **13**, 192 (2018).
[56] J. Bommer, H. Zhang, Ö. Gül, B. Nijholt, M. Wimmer, F. Rybakov, J. Garaud, D. Rodic, E. Babaev, M. Troyer, D. Car, S. Plissard, E. Bakkers, K. Watanabe, T. Taniguchi, and L. Kouwenhoven, Spin-Orbit Protection of Induced Superconductivity in Majorana Nanowires, Phys. Rev. Lett. **122**, 187702 (2019).
[57] H. Zhang, M. W. A. de Moor, J. D. S. Bommer, D. Xu, G. Wang, N. van Loo, C.-X. Liu, S. Gazibegovic, J. A. Logan, D. Car, R. L. M. O. het Veld, P. J. van Veldhoven, S. Koelling, M. A. Verheijen, M. Pendharkar, D. J. Pennachio, B. Shojaei, J. S. Lee, C. J. Palmstrøm, E. P. A. M. Bakkers, S. D. Sarma, and L. P. Kouwenhoven, Large Zero-Bias Peaks in InSb-Al Hybrid Semiconductor-Superconductor Nanowire Devices, arXiv:2101.11456 [cond-mat] (2021).
[58] A. Grivnin, E. Bor, M. Heiblum, Y. Oreg, and H. Shtrikman, Concomitant Opening of a Bulk-Gap with an Emerging Possible Majorana Zero Mode, Nat. Commun. **10**, 1940 (2019).
[59] D. Puglia, E. A. Martinez, G. C. Ménard, A. Pöschl, S. Gronin, G. C. Gardner, R. Kallaher, M. J. Manfra, C. M. Marcus, A. P. Higginbotham, and L. Casparis, Closing of the induced gap in a hybrid superconductor-semiconductor nanowire, Phys. Rev. B **103**, 235201 (2021).
[60] S. Heedt, M. Quintero-Pérez, F. Borsoi, A. Fursina, N. van Loo, G. P. Mazur, M. Nowak, M. Ammerlaan, K. Li, S. Korneychuk, J. Shen, M. A. Y. van de Poll, G. Badawy, S. Gazibegovic, N. de Jong, P. Aseev, K. van Hoogdalem, E. P. A. M. Bakkers, and L. P. Kouwenhoven, Shadow-wall lithography of ballistic superconductor–semiconductor quantum devices, Nat. Commun. **12**, 4914 (2021).
[61] L. Rokhinson, X. Liu, and J. Furdyna, The Fractional a.c. Josephson Effect in a Semiconductor-Superconductor Nanowire as a Signature of Majorana Particles, Nat. Phys. **8**, 795 (2012).
[62] D. Laroche, D. Bouman, D. van Woerkom, A. Proutski, C. Murthy, D. Pikulin, C. Nayak, R. van Gulik, J. Nygård, P. Krogstrup, L. Kouwenhoven, and A. Geresdi, Observation of the 4π-Periodic Josephson Effect in Indium Arsenide Nanowires, Nat. Commun. **10**, 245 (2019).
[63] M. Dartiailh, W. Mayer, J. Yuan, K. Wickramasinghe, A. Matos-Abiague, I. Žutić, and J. Shabani, Phase Signature of Topological Transition in Josephson Junctions, Phys. Rev. Lett. **126**, 036802 (2021).
[64] A. Higginbotham, S. Albrecht, G. Kiršanskas, W. Chang, F. Kuemmeth, P. Krogstrup, T. Jespersen, J. Nygård, K. Flensberg, and C. Marcus, Parity Lifetime of Bound States in a Proximitized Semiconductor Nanowire, Nat. Phys. **11**, 1017 (2015).
[65] S. Albrecht, A. Higginbotham, M. Madsen, F. Kuemmeth, T. Jespersen, J. Nygård, P. Krogstrup, and C. Marcus, Exponential Protection of Zero Modes in Majorana Islands, Nature **531**, 206 (2016).
[66] S. Albrecht, E. Hansen, A. Higginbotham, F. Kuemmeth, T. Jespersen, J. Nygård, P. Krogstrup, J. Danon, K. Flensberg, and C. Marcus, Transport Signatures of Quasiparticle Poisoning in a Majorana Island, Phys. Rev. Lett. **118**, 137701 (2017).
[67] J. Shen, S. Heedt, F. Borsoi, B. van Heck, S. Gazibegovic, R. Op het Veld, D. Car, J. Logan, M. Pendharkar, S. Ramakers, G. Wang, D. Xu, D. Bouman, A. Geresdi, C. Palmstrøm, E. Bakkers, and L. Kouwenhoven, Parity Transitions in the Superconducting Ground State of Hybrid InSb–Al Coulomb Islands, Nat. Commun. **9**, 4801 (2018).
[68] S. Vaitiekėnas, G. Winkler, B. van Heck, T. Karzig, M.-T. Deng, K. Flensberg, L. Glazman, C. Nayak, P. Krogstrup, R. Lutchyn, and C. Marcus, Flux-Induced Topological Superconductivity in Full-Shell Nanowires, Science **367**, eaav3392 (2020).
[69] M. De Moor, J. Bommer, D. Xu, G. Winkler, A. Antipov, A. Bargerbos, G. Wang, N. Loo, R. Op Het Veld, S. Gazibegovic, D. Car, J. Logan, M. Pendharkar, J. Lee, E. M Bakkers, C. Palmstrom, R. Lutchyn, L. Kouwenhoven, and H. Zhang, Electric Field Tunable Superconductor-Semiconductor Coupling in Majorana Nanowires, New J. Phys. **20**, 103049 (2018).
[70] J. Chen, B. Woods, P. Yu, M. Hocevar, D. Car, S. Plissard, E. Bakkers, T. Stanescu, and S. Frolov, Ubiquitous Non-Majorana Zero-Bias Conductance Peaks in Nanowire Devices, Phys. Rev. Lett. **123**, 107703 (2019).
[71] G. Anselmetti, E. Martinez, G. Ménard, D. Puglia, F. Malinowski, J. Lee, S. Choi, M. Pendharkar, C. Palmstrøm, C. Marcus, L. Casparis, and A. Higginbotham, End-to-End Correlated Subgap States in Hybrid Nanowires, Phys. Rev. B **100**, 205412 (2019).
[72] G. Ménard, G. Anselmetti, E. Martinez, D. Puglia, F. Malinowski, J. Lee, S. Choi, M. Pendharkar, C. Palmstrøm, K. Flensberg, C. Marcus, L. Casparis, and A. Higginbotham, Conductance-Matrix Symmetries of a Three-Terminal Hybrid Device, Phys. Rev. Lett. **124**, 036802 (2020).
[73] C. Jünger, R. Delagrange, D. Chevallier, S. Lehmann, K. Dick, C. Thelander, J. Klinovaja, D. Loss, A. Baumgartner, and C. Schönenberger, Magnetic-Field-Independent Subgap States in Hybrid Rashba Nanowires, Phys. Rev. Lett. **125**, 017701 (2020).

[74] P. Yu, J. Chen, M. Gomanko, G. Badawy, E. Bakkers, K. Zuo, V. Mourik, and S. Frolov, Non-Majorana States Yield Nearly Quantized Conductance in Proximatized Nanowires, Nat. Phys. **17**, 482 (2021).

[75] M. Valentini, F. Peñaranda, A. Hofmann, M. Brauns, R. Hauschild, P. Krogstrup, P. San-Jose, E. Prada, R. Aguado, and G. Katsaros, Nontopological zero-bias peaks in full-shell nanowires induced by flux-tunable Andreev states, Science **373**, 82 (2021).

[76] E. Prada, P. San-Jose, M. de Moor, A. Geresdi, E. Lee, J. Klinovaja, D. Loss, J. Nygård, R. Aguado, and L. Kouwenhoven, From Andreev to Majorana Bound States in Hybrid Superconductor–Semiconductor Nanowires, Nat. Rev. Phys. **2**, 575 (2020).

[77] J. Liu, A. C. Potter, K. T. Law, and P. A. Lee, Zero-Bias Peaks in the Tunneling Conductance of Spin-Orbit-Coupled Superconducting Wires with and without Majorana End-States, Phys. Rev. Lett. **109**, 267002 (2012).

[78] D. Pikulin, J. Dahlhaus, M. Wimmer, H. Schomerus, and C. Beenakker, A Zero-Voltage Conductance Peak from Weak Antilocalization in a Majorana Nanowire, New J. Phys. **14**, 125011 (2012).

[79] D. Bagrets and A. Altland, Class D Spectral Peak in Majorana Quantum Wires, Phys. Rev. Lett. **109**, 227005 (2012).

[80] D. Roy, N. Bondyopadhaya, and S. Tewari, Topologically Trivial Zero-Bias Conductance Peak in Semiconductor Majorana Wires from Boundary Effects, Phys. Rev. B **88**, 020502 (2013).

[81] T. D. Stanescu and S. Tewari, Disentangling Majorana Fermions from Topologically Trivial Low-Energy States in Semiconductor Majorana Wires, Phys. Rev. B **87**, 140504 (2013).

[82] H. Pan and S. Das Sarma, Physical Mechanisms for Zero-Bias Conductance Peaks in Majorana Nanowires, Phys. Rev. Research **2**, 013377 (2020).

[83] H. Pan, W. S. Cole, J. D. Sau, and S. Das Sarma, Generic Quantized Zero-Bias Conductance Peaks in Superconductor-Semiconductor Hybrid Structures, Phys. Rev. B **101**, 024506 (2020).

[84] S. Das Sarma and H. Pan, Disorder-induced zero-bias peaks in Majorana nanowires, Phys. Rev. B **103**, 195158 (2021).

[85] H. Pan and S. Das Sarma, Disorder Effects on Majorana Zero Modes: Kitaev Chain versus Semiconductor Nanowire, Phys. Rev. B **103**, 224505 (2021).

[86] H. Pan and S. Das Sarma, Crossover between Trivial Zero Modes in Majorana Nanowires, Phys. Rev. B **104**, 054510 (2021).

[87] H. Pan, J. D. Sau, and S. Das Sarma, Three-Terminal Nonlocal Conductance in Majorana Nanowires: Distinguishing Topological and Trivial in Realistic Systems with Disorder and Inhomogeneous Potential, Phys. Rev. B **103**, 014513 (2021).

[88] H. Pan, C.-X. Liu, M. Wimmer, and S. Das Sarma, Quantized and Unquantized Zero-Bias Tunneling Conductance Peaks in Majorana Nanowires: Conductance below and above 2 e 2 / h, Phys. Rev. B **103**, 214502 (2021).

[89] T. D. Stanescu and S. Tewari, Nonlocality of Zero-Bias Anomalies in the Topologically Trivial Phase of Majorana Wires, Phys. Rev. B **89**, 220507 (2014).

[90] B. D. Woods, J. Chen, S. M. Frolov, and T. D. Stanescu, Zero-Energy Pinning of Topologically Trivial Bound States in Multiband Semiconductor-Superconductor Nanowires, Phys. Rev. B **100**, 125407 (2019).

[91] G. Kells, D. Meidan, and P. W. Brouwer, Near-Zero-Energy End States in Topologically Trivial Spin-Orbit Coupled Superconducting Nanowires with a Smooth Confinement, Phys. Rev. B **86**, 100503 (2012).

[92] E. Prada, P. San-Jose, and R. Aguado, Transport Spectroscopy of N S Nanowire Junctions with Majorana Fermions, Phys. Rev. B **86**, 180503 (2012).

[93] C.-X. Liu, J. D. Sau, T. D. Stanescu, and S. Das Sarma, Andreev Bound States versus Majorana Bound States in Quantum Dot-Nanowire-Superconductor Hybrid Structures: Trivial versus Topological Zero-Bias Conductance Peaks, Phys. Rev. B **96**, 075161 (2017).

[94] F. Peñaranda, R. Aguado, P. San-Jose, and E. Prada, Quantifying Wave-Function Overlaps in Inhomogeneous Majorana Nanowires, Phys. Rev. B **98**, 235406 (2018).

[95] C. Moore, T. D. Stanescu, and S. Tewari, Two-Terminal Charge Tunneling: Disentangling Majorana Zero Modes from Partially Separated Andreev Bound States in Semiconductor-Superconductor Heterostructures, Phys. Rev. B **97**, 165302 (2018).

[96] J. Avila, F. Peñaranda, E. Prada, P. San-Jose, and R. Aguado, Non-Hermitian Topology as a Unifying Framework for the Andreev versus Majorana States Controversy, Commun. Phys. **2**, 133 (2019).

[97] A. Vuik, B. Nijholt, A. R. Akhmerov, and M. Wimmer, Reproducing Topological Properties with Quasi-Majorana States, SciPost Phys. **7**, 061 (2019).

[98] T. Stanescu and S. Tewari, Robust Low-Energy Andreev Bound States in Semiconductor-Superconductor Structures: Importance of Partial Separation of Component Majorana Bound States, Phys. Rev. B **100**, 155429 (2019).

[99] F. Setiawan, C.-X. Liu, J. D. Sau, and S. Das Sarma, Electron Temperature and Tunnel Coupling Dependence of Zero-Bias and Almost-Zero-Bias Conductance Peaks in Majorana Nanowires, Phys. Rev. B **96**, 184520 (2017).

[100] A. Ptok, A. Kobiałka, and T. Domański, Controlling the Bound States in a Quantum-Dot Hybrid Nanowire, Phys. Rev. B **96**, 195430 (2017).

[101] C. Moore, C. Zeng, T. D. Stanescu, and S. Tewari, Quantized Zero-Bias Conductance Plateau in Semiconductor-Superconductor Heterostructures without Topological Majorana Zero Modes, Phys. Rev. B **98**, 155314 (2018).

[102] C.-X. Liu, J. D. Sau, and S. Das Sarma, Distinguishing Topological Majorana Bound States from Trivial Andreev Bound States: Proposed Tests through Differential Tunneling Conductance Spectroscopy, Phys. Rev. B **97**, 214502 (2018).

[103] C. Reeg, O. Dmytruk, D. Chevallier, D. Loss, and J. Klinovaja, Zero-Energy Andreev Bound States from Quantum Dots in Proximitized Rashba Nanowires, Phys. Rev. B **98**, 245407 (2018).

[104] Y. Huang, H. Pan, C.-X. Liu, J. D. Sau, T. D. Stanescu, and S. Das Sarma, Metamorphosis of Andreev Bound States into Majorana Bound States in Pristine Nanowires, Phys. Rev. B **98**, 144511 (2018).

[105] Y.-H. Lai, J. D. Sau, and S. Das Sarma, Presence versus Absence of End-to-End Nonlocal Conductance Correlations in Majorana Nanowires: Majorana Bound States versus Andreev Bound States, Phys. Rev. B **100**, 045302 (2019).

[106] G. Sharma, C. Zeng, T. D. Stanescu, and S. Tewari, Hybridization Energy Oscillations of Majorana and Andreev Bound States in Semiconductor-Superconductor Nanowire Heterostructures, Phys. Rev. B **101**, 245405 (2020).

[107] R. Hess, H. F. Legg, D. Loss, and J. Klinovaja, Local and Nonlocal Quantum Transport Due to Andreev Bound States in Finite Rashba Nanowires with Superconducting and Normal Sections, Phys. Rev. B **104**, 075405 (2021).

[108] D. Chevallier, D. Sticlet, P. Simon, and C. Bena, Mutation of Andreev into Majorana Bound States in Long Superconductor-Normal and Superconductor-Normal-Superconductor Junctions, Phys. Rev. B **85**, 235307 (2012).

[109] J. Cayao, E. Prada, P. San-Jose, and R. Aguado, SNS Junctions in Nanowires with Spin-Orbit Coupling: Role of Confinement and Helicity on the Subgap Spectrum, Phys. Rev. B **91**, 024514 (2015).

[110] C. Fleckenstein, F. Domínguez, N. Traverso Ziani, and B. Trauzettel, Decaying Spectral Oscillations in a Majorana Wire with Finite Coherence Length, Phys. Rev. B **97**, 155425 (2018).

[111] Z.-G. Liu, Y.-X. Huang, G.-C. Guo, and M. Gong, Majorana and Non-Majorana Modes in a Nanowire in Partially Proximity to a Superconductor, J. Appl. Phys. **129**, 094301 (2021).

[112] Z. Cao, H. Zhang, H.-F. Lü, W.-X. He, H.-Z. Lu, and X. C. Xie, Decays of Majorana or Andreev Oscillations Induced by Steplike Spin-Orbit Coupling, Phys. Rev. Lett. **122**, 147701 (2019).

[113] C. Zeng, G. Sharma, T. D. Stanescu, and S. Tewari, Feasibility of Measurement-Based Braiding in the Quasi-Majorana Regime of Semiconductor-Superconductor Heterostructures, Phys. Rev. B **102**, 205101 (2020).

[114] J. Klinovaja and D. Loss, Composite Majorana Fermion Wave Functions in Nanowires, Phys. Rev. B **86**, 085408 (2012).

[115] S. Das Sarma, J. D. Sau, and T. D. Stanescu, Splitting of the Zero-Bias Conductance Peak as Smoking Gun Evidence for the Existence of the Majorana Mode in a Superconductor-Semiconductor Nanowire, Phys. Rev. B **86**, 220506 (2012).

[116] D. Rainis, L. Trifunovic, J. Klinovaja, and D. Loss, Towards a Realistic Transport Modeling in a Superconducting Nanowire with Majorana Fermions, Phys. Rev. B **87**, 024515 (2013).

[117] T. Stanescu, R. Lutchyn, and S. Das Sarma, Dimensional Crossover in Spin-Orbit-Coupled Semiconductor Nanowires with Induced Superconducting Pairing, Phys. Rev. B **87**, 094518 (2013).

[118] T. D. Stanescu, S. Tewari, J. D. Sau, and S. Das Sarma, To Close or Not to Close: The Fate of the Superconducting Gap Across the Topological Quantum Phase Transition in Majorana-Carrying Semiconductor Nanowires, Phys. Rev. Lett. **109**, 266402 (2012).

[119] R. V. Mishmash, D. Aasen, A. P. Higginbotham, and J. Alicea, Approaching a Topological Phase Transition in Majorana Nanowires, Phys. Rev. B **93**, 245404 (2016).

[120] T. Stanescu, J. Sau, R. Lutchyn, and S. Das Sarma, Proximity Effect at the Superconductor-Topological Insulator Interface, Phys. Rev. B **81**, 241310 (2010).

[121] T. D. Stanescu and S. Das Sarma, Proximity-induced low-energy renormalization in hybrid semiconductor-superconductor Majorana structures, Phys. Rev. B **96**, 014510 (2017).

[122] A. Kitaev, Periodic table for topological insulators and superconductors, AIP Conf. Proc. **1134**, 22 (2009).

[123] A. P. Schnyder, S. Ryu, A. Furusaki, and A. W. W. Ludwig, Classification of Topological Insulators and Superconductors, AIP Conf. Proc. **1134**, 10 (2009).

[124] S. Ryu, A. Schnyder, A. Furusaki, and A. Ludwig, Topological Insulators and Superconductors: Tenfold Way and Dimensional Hierarchy, New J. Phys. **12**, 065010 (2010).

[125] C.-K. Chiu, J. C. Y. Teo, A. P. Schnyder, and S. Ryu, Classification of topological quantum matter with symmetries, Rev. Mod. Phys. **88**, 035005 (2016).

[126] P. Marra, Data and code for "Majorana/Andreev crossover and the fate of the topological phase transition in inhomogeneous nanowires", Zenodo, 10.5281/zenodo.5725493 (2021).

[127] P. Marra, D. Inotani, and M. Nitta, 1D Majorana Goldstinos and extended supersymmetry in quantum wires, arXiv:2106.09039 [cond-mat] (2021).

[128] P. Marra, D. Inotani, and M. Nitta, Dispersive 1D Majorana modes with emergent supersymmetry in 1D proximitized superconductors via spatially-modulated potentials and magnetic fields, arXiv:2106.09047 [cond-mat] (2021).

[129] D. Sticlet, C. Bena, and P. Simon, Spin and Majorana Polarization in Topological Superconducting Wires, Phys. Rev. Lett. **108**, 096802 (2012).

[130] S.-Q. Shen, Topological insulators Dirac equation in condensed matters (Springer, 2017).

[131] J. C. Budich and E. Ardonne, Equivalent topological invariants for one-dimensional Majorana wires in symmetry class *D*, Phys. Rev. B **88**, 075419 (2013).

[132] M. Wimmer, Algorithm 923: Efficient Numerical Computation of the Pfaffian for Dense and Banded Skew-Symmetric Matrices, ACM Trans. Math. Softw. **38**, 30 (2012).

[133] A. Grabsch, Y. Cheipesh, and C. W. J. Beenakker, Pfaffian Formula for Fermion Parity Fluctuations in a Superconductor and Application to Majorana Fusion Detection, Ann. Phys. **531**, 1900129 (2019).

[134] B. Zocher and B. Rosenow, Modulation of Majorana-Induced Current Cross-Correlations by Quantum Dots, Phys. Rev. Lett. **111**, 036802 (2013).

[135] J. Liu, F.-C. Zhang, and K. T. Law, Majorana Fermion Induced Nonlocal Current Correlations in Spin-Orbit Coupled Superconducting Wires, Phys. Rev. B **88**, 064509 (2013).

[136] J. Li, T. Yu, H.-Q. Lin, and J. Q. You, Probing the non-locality of Majorana fermions via quantum correlations, Sci. Rep. **4**, 4930 (2014).

[137] A. Haim, E. Berg, F. von Oppen, and Y. Oreg, Current Correlations in a Majorana Beam Splitter, Phys. Rev. B **92**, 245112 (2015).

[138] A. Haim, E. Berg, F. von Oppen, and Y. Oreg, Signatures of Majorana Zero Modes in Spin-Resolved Current Correlations, Phys. Rev. Lett. **114**, 166406 (2015).

[139] D. J. Clarke, Experimentally Accessible Topological Quality Factor for Wires with Zero Energy Modes, Phys. Rev. B **96**, 201109 (2017).

[140] A. Schuray, L. Weithofer, and P. Recher, Fano Resonances in Majorana Bound States–Quantum Dot Hybrid Systems, Phys. Rev. B **96**, 085417 (2017).

[141] E. Prada, R. Aguado, and P. San-Jose, Measuring Majorana Nonlocality and Spin Structure with a Quantum Dot, Phys. Rev. B **96**, 085418 (2017).

[142] T. Rosdahl, A. Vuik, M. Kjaergaard, and A. Akhmerov, Andreev Rectifier: A Nonlocal Conductance Signature of Topological Phase Transitions, Phys. Rev. B **97**, 045421 (2018).

[143] M. Hell, K. Flensberg, and M. Leijnse, Distinguishing Majorana Bound States from Localized Andreev Bound States by Interferometry, Phys. Rev. B **97**, 161401 (2018).

[144] L. S. Ricco, M. de Souza, M. S. Figueira, I. A. Shelykh, and A. C. Seridonio, Spin-Dependent Zero-Bias Peak in a Hybrid Nanowire-Quantum Dot System: Distinguishing Isolated Majorana Fermions from Andreev Bound States, Phys. Rev. B **99**, 155159 (2019).

[145] O. A. Awoga, J. Cayao, and A. M. Black-Schaffer, Supercurrent Detection of Topologically Trivial Zero-Energy States in Nanowire Junctions, Phys. Rev. Lett. **123**, 117001 (2019).

[146] R. V. Mishmash, B. Bauer, F. von Oppen, and J. Alicea, Dephasing and Leakage Dynamics of Noisy Majorana-Based Qubits: Topological versus Andreev, Phys. Rev. B **101**,

075404 (2020).
[147] J. Cayao and A. M. Black-Schaffer, Distinguishing Trivial and Topological Zero-Energy States in Long Nanowire Junctions, Phys. Rev. B **104**, L020501 (2021).
[148] X. Cai, L.-J. Lang, S. Chen, and Y. Wang, Topological Superconductor to Anderson Localization Transition in One-Dimensional Incommensurate Lattices, Phys. Rev. Lett. **110**, 176403 (2013).
[149] W. Degottardi, D. Sen, and S. Vishveshwara, Majorana Fermions in Superconducting 1D Systems Having Periodic, Quasiperiodic, and Disordered Potentials, Phys. Rev. Lett. **110**, 146404 (2013).
[150] W. Degottardi, M. Thakurathi, S. Vishveshwara, and D. Sen, Majorana Fermions in Superconducting Wires: Effects of Long-Range Hopping, Broken Time-Reversal Symmetry, and Potential Landscapes, Phys. Rev. B **88**, 165111 (2013).
[151] P. Marra and M. Nitta, Topologically nontrivial Andreev bound states, Phys. Rev. B **100**, 220502 (2019).